Mountain Rescue Helicopter Design Proposal
For
The American Helicopter Society

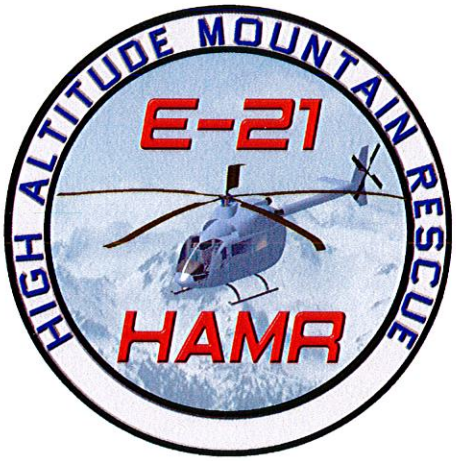

By
Infinity Aerospace
Embry-Riddle Aeronautical University
Prescott Arizona
May 4, 2004

Team Members:
Courtney Balzer
Bret Davenport
Anthony Gold
Aaron Hrdlichka
John Patterson
John Plets
Joseph Roop
Kenneth Young

Written and Edited by

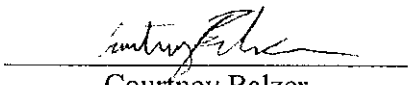

Courtney Balzer

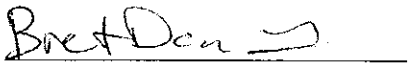

Bret Davenport

Anthony Gold

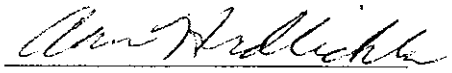

Aaron Hrdlichka

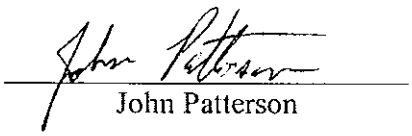

John Patterson

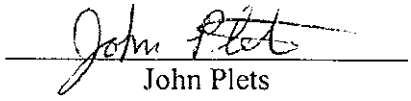

John Plets

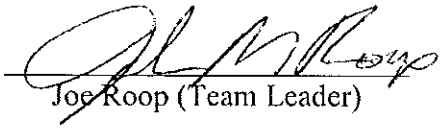

Joe Roop (Team Leader)

Kenneth Young

TABLE OF CONTENTS

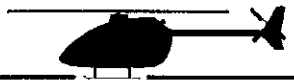

LIST OF FIGURES

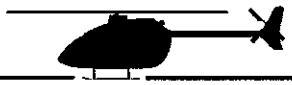

LIST OF TABLES

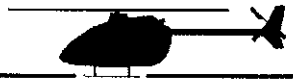

LIST OF SYMBOLS / ABBREVIATIONS

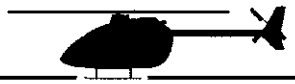

Abbreviations

AEP ..... Aircraft Estimated Price
AHS ..... American Helicopter Society
CEF ..... Cost Escalation Factor
CFR ..... Code of Federal Regulations
DL ..... Disk Loading
DMS ..... Defense Marketing Services
DOC ..... Direct Operating Cost
EO ..... Electro Optical
IA ..... Infinity Aerospace
FLIR ..... Forward Looking Infrared
FM ..... Figure of Merit
GW ..... Gross Weight
HAMR ..... High Altitude Mountain Rescue
HOGE ..... Hover Out of Ground Effect
IFR ..... Instrument Flight Rules
ISA ..... International Standard Atmosphere
JAR ..... Joint Aviation Regulations
MGW ..... Maximum Gross Weight
Nm ..... Number of Aircraft Produced
OEI ..... One Engine Out
Rbl ..... Block Distance
RTDE ..... Research Test Design Evaluation
SFC ..... Specific Fuel Consumption
SHP ..... Shaft Horsepower
UL ..... Useful Load

Symbols

A1 ..... Lateral Cyclic (Swashplate) (+ Tilt Right)
a_{1s} ..... Longitudinal Flapping Angle (+ Forward Flap Up)
B1 ..... Longitudinal Cyclic (Swashplate) (+ Tilt Forward)
b_{1s} ..... Lateral Flapping Angle (+ Right Flap Down)
D_v ..... Vertical Drag on Helicopter
C_{adem} ..... Airframe Engineering And Design Cost
C_{aedr} ..... Airframe Engineering Design Cost
C_{apcm} ..... Airplane Production Cost
C_{dstr} ..... Design Support And Testing Cost
C_{finm} ..... Finance Of Manufacturing Program
C_{finr} ..... Cost To Finance RTDE Cost
C_{ftar} ..... Flight Test Aircraft Cost

C_{ftom} ..... Production Flight Test Cost
C_{ftor} ..... Flight Test Operations Cost
C_{pro} ..... Profit Cost
C_{pror} ..... Profit
C_{tsfr} ..... Test Simulation Facilities Cost
D_M ..... Diameter Of The Main Rotor
D_T ..... Diameter Of The Main Rotor
P_c ..... Power to Cruise
P_h ..... Power to Hover
hp ..... Horsepower
lb ..... Pounds Force
sfc ..... Specific Horsepower
shp ..... Shaft Horsepower

ρ ..... Air Density
Θ ..... Longitudinal Body Angle (+ Pitch Up)

1.0 INTRODUCTION

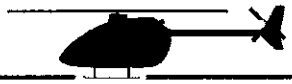

1.1 Report Layout

This is Infinity Aerospace's (IA) preliminary design report number two of two. The first report "AE 420 Aircraft Design Report: Mission Weight Sizing, Take-off Weight Sensitivities and Performance Constraint Analysis for the IA Helicopter" resulted in an initial estimation of the size and power required in order to meet the AHS mission specifications (See Appendix A). The purpose of this report is to cover a more detailed analysis of the following:

- Layout and ergonomics of cabin
- Propulsion system and power consumption at various flight regimes
- Layout and design of main rotor
- Layout and design of tail rotor
- Landing gear
- Weight Estimates of payload weights and take-off weight sensitivity.
- Trim ability analysis equivalent of stability analysis
- Fuselage drag analysis
- Three View
- A market analysis exploring the rescue helicopter market as well as the proposed price and number of helicopters planned to produce
- This report will close with conclusions, recommendations, and mission verifications of the design team.

1.2 Mission Specifications

The role of the E-21 helicopter is to perform mountain rescue operations at high altitude. The E-21 helicopter must be capable of performing a mission consisting of take off from 6000-ft Hd, 1 hour outbound leg with a crew of 4 at 140 knots, 20 minutes on station for hoist operations with recovery of 2 patients at 12000-ft Hd, and 1 hour return leg at 140 knots. The helicopter must be capable of operation in snow.

The helicopters payload consists of medical and search equipment along with passengers and backup power. The E-21 is designed for a crew of 4, 2 patients, and carries a host of medical equipment.

The E-21 helicopter must be capable of one engine inoperative (OEI) hover out of ground effect (HOGE) at maximum gross weight (MGW) up to 12000-ft Hd, International Standard Atmosphere (ISA). The IA must be able to HOGE with all engines operative at MGW up to 15000-ft Hd, ISA. The anti-torque system must be capable of maintaining heading in hover with wind from any azimuth up to at least 40 knots at 15000-ft Hd. The E-21 needs to have a range of 280 nautical miles. The maximum speed of the IA needs to be 145 knots.

2.0 HELICOPTER CONFIGURATION

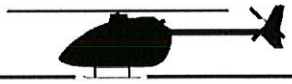

The aircraft configuration was highly dependent on the mission specifications given by AHS. Historical trends of other helicopters were researched to determine the general configuration, sizing, and layout of helicopters used for search and rescue operations. The basic configuration of one main rotor and one tail rotor was chosen because IA did not need the size of 2 main rotors and this configuration best fits the mission specs. To accomplish hover out of ground effect (HOGE) at 12,000-ft Hd, 3 engines were chosen to give the E-21 enough horsepower for this requirement. A conventional tail rotor was chosen due to the need to hover with a 40-kt crosswind. The conventional tail rotor configuration was the most effective with the least horsepower required; this configuration allowed the E-21 to save horsepower for hovering. The tail boom and rotor were placed high for blade clearance and to allow for the use of the aft entry door. The configuration layout of the E-21 was also highly dependent on the stability and trim calculations. The overall configuration can be seen in the three-view section.

2.1 Layout and Design of the Fuselage and Cabin

The layout and design of the cabin was due mainly to the weight and balance and the ergonomics of the search and rescue mission. The cabin sizing was driven by the spacing needed for 2 patients in litters and 2 crew members attending to the patients with all the required medical equipment. Many configurations were laid out with scaled models establish the spacing was needed for a static configuration with all patients and crew locked in. The cabin configurations were also dependent on the ergonomics of hoisting patients on litters into the cabin and caring for them en route. Statically, the cabin must be 6-ft wide and have a length of 10-ft, with the crew seats next to the cabin and the patients in the litters placed lengthwise along the cabin, shown in Appendix D. This 6-ft cabin width gives the crew members ample room to treat any part of the patient's bodies.

The hoist placement was crucial in the ergonomics of the rescue operation. The hoist was placed on a 3-ft arm that can swivel towards the fuselage. The swiveling hoist allows for one crew member to stand on the skid and direct the litter into the cabin more easily than a with a stationary hoist arm. After the outside crew member has moved the litter partially into the cabin, the other crew member can then maneuver the patient into the proper position in the cabin. Due to the high weight of the hoist, the medical equipment was placed in a configuration to even out the lateral CG. All equipment positions can be seen in Table 14.2 in Appendix B.

The final dimensions of the fuselage came to 20-ft long, 6-ft wide, and 9-ft high. The dimensions coincide with the sizing of similar designs of helicopters, such as the EC-145. The nose of the fuselage was sized for equipment placement and field of view. The first 2-ft of the nose were sized to carry avionics and weather radar. The next four feet of the nose were design for the spacing of the pilots, controls, displays, and other avionics. The undercarriage of the fuselage was designed for fuel tanks, structure, and other equipment. The undercarriage sizing was derived to have a height of 1-ft. The next 10-ft following

the cockpit was sized for the cabin, which is described above. The 4-ft after the cabin is tapered for extra cabin space and the aft entry doors for easy loading and unloading during ground operations.

2.2 Field of View Analysis

The field of view is extensive for helicopter pilots during normal flight regimens. During search and rescue missions helicopter pilots need to be able to see a broader area for hovering and winching a patient. Some flights will require the pilot to fly in close proximity of ground obstructions, so the more the pilot can see the safer the rescue mission can be. The field of view for the E-21 was designed to give the pilot a wide viewing range. The front and right field of view of the E-21 can be seen in Figure 2-1 and Figure 2-2.

Figure 2-1 - Front Field Of View

Figure 2-2 - Right Field Of View

The interior and exterior layout and design of the E-21 HAMR was based upon two very successful search and rescue helicopter designs; McDonnell Douglas MD 900 Explorer and the Eurocopter EC 145. Many of the HAMR's design features are standard components to search and rescue helicopters. The overall shape of the HAMR was also based on the two aforementioned designs. This was to keep the HAMR as aerodynamically clean as possible for less drag at cruise velocities. The cabin was made larger then other rescue helicopters so that in flight EMT work could be accomplished. The larger cabin also allows for two litters to be extracted and secured from hostile environments. The rear clamshell type door is to accommodate ground crew for easy patient extraction. The cockpit will be fitted with a "glass" cockpit digital interface that will incorporate digital fly-by-wire flight control technology to save weight. The cockpit is also larger then industry competitive aircraft to give the pilots more room to work. The cabin structure will be larger to accommodate for the added weight of the third engine overhead.

2.3 Conclusions and Recommendations

The conventional helicopter configuration was chosen because it best meets the needs of IA's search and rescue mission. The cabin was laid out due to the mission's ergonomics of loading of and tending to the patients. The fuselage was derived by finding the most practical places for all the equipment and other parts.

3.0 PROPULSION SYSTEM

3.1 Engine

The IA E-21 is powered by three LHTEC T800-LHT-800 engines. The LHTEC T800-LHT-800 engine was developed to meet the requirements of the Army's LHX helicopter, now the Sikorsky/Boeing Comanche, and was FAA certified in 1993. Table 3.1 below lists the specifications of the LHTEC T800-LHT-800 engines.

Table 3.1 - LHTEC T800-LHT-800 Specifications

Dimensions		Performance	
Length overall	33.8 in	Contingency	1,399 shp
Width overall	22.2 in	Max (Normal Use)	1,334 shp
Height overall	26.8 in	Intermediate (30 min)	1,239 shp
sfc	0.450	Continuous	1,038 shp

The engines are arranged behind the mast and above the cabin of the E-21 as shown in Appendix C. The face of the center engine is 47.8-in aft of the mast axis. The faces of the two lateral engines are 23.8-in aft of the mast axis and the centerlines of the two lateral engines are 27.2-in to either side of the mast axis. The precise placement of the engines was determined with weight and balance while taking into consideration inlet ducts, transmission compatibility, tail rotor shaft clearance, and main rotor flapping clearance. The engine power is transmitted to the main and tail rotors through the transmission as shown in Appendix C.

It was initially assumed that by meeting the power requirements for the OEI HOGE at 12,000-ft Hd AHS specification the E-21 would be able to meet all other performance specifications because the total power installation required for such a specification exceeds by a factor of 0.5 the power installed on similar rotorcraft. This assumption was verified once the analyses for hover and cruise were completed. Hover at 12,000-ft Hd was found to require 1,440-hp and cruise at 145-kts at 12,000-ft Hd was found to require 1,130-hp. Therefore, the engine type and number selection was largely based on the ability of the engine to meet the power requirements of OEI HOGE at 12,000-ft Hd. Along with the above consideration were the following four requirements: advanced technology, low sfc, light weight, and high power to weight ratio.

A three-engine configuration was chosen over a two-engine configuration because the OEI HOGE at 12,000-ft Hd AHS specification requires the E-21 to operate at low throttle settings during normal operations, increasing the sfc as illustrated in Figure 3-1. Due to

the large amount of excessive power installed on the E-21, having only two engines would exacerbate this problem by increasing the total power installed by a factor of 0.33 compared to the three-engine configuration.

As stated above the power required to hover OGE at 12,000-ft Hd was determined to be 1,440-hp. However, due to altitude effects this translates into 2,168-hp at sea level. This total power was found by adding the six following power consumers on a helicopter: main rotor power, tail rotor power, generator power, hydraulic power, transmission losses for each of the above, and an installation loss factor. The main rotor power requirement was determined to be 1,160-hp at 12,000-ft Hd. The tail rotor power requirement was determined to be 138-hp at 12,000-ft Hd with a 40-kts crosswind in the most critical azimuth. The generator power was calculated to be 15-hp. The hydraulic system power was estimated to be 10-hp. The transmission losses were determined to be 43-hp using Prouty's (2002) methods for calculating power losses from friction in gear transmission systems. Installation losses accounted for 66-hp and were determined from an installation loss factor that was produced by adding assumed values for common installation losses. These assumed values were picked from a table in Prouty that listed the typical ranges for installation losses in helicopters.

3.2 Fuel

3.2.1 Power Setting

Before one can find the sfc and, therefore, the fuel consumption for a given flight regime, one must know the power setting, because sfc is a function of the power setting for a turbine engine. Power setting is a function of required power output, altitude, and Mach number. Therefore, altitude and Mach number must be taken into account when trying to find the correct power setting for a given altitude, Mach number, and required power output. The power setting is necessary to calculate fuel consumption using sfc because sfc is a function of power setting for a turbine engine. Though the power of the AIAA Generic Small Turbo-Shaft Engine (rubber engine) exceeded the power of the LHTEC T800-LHT-800 by 45% its data was used to find trends that would allow IA to predict sfc because no such data could be found from the manufacturer. Therefore, the power setting for different flight regimes was found using trends from the rubber engine. First, rubber engine horsepower data was extrapolated to 16,000-ft Hd. Second, power setting vs. power was graphed in MS Excel for M=0 from 0 - 16,000-ft Hd in 4,000-ft Hd increments and for M=0.3 from 0 - 16,000-ft Hd in 4,000-ft increments. From these graphs trend line equations were obtained. Third, the power required, altitude, and Mach number were obtained for a flight regime. Fourth, a power setting was interpolated with respect to altitude from the trend line equations for M=0, and a power setting was interpolated with respect to altitude from the trend line equations for M=0.3. Fifth, the two altitude power settings were then interpolated with respect to the flight Mach number to obtain a final power setting.

3.2.2 SFC

The sfc for the LHTEC T800-LHT-800 was determined for different flight regimes by interpolating between the two trend lines in Figure 3-1 with respect to Mach number and then subtracting 0.012 to account for the difference between full throttle sfc of the rubber engine and the LHTEC T800-LHT-800. The trend lines were obtained from plotting the sfc vs. the power output in percent from the AIAA Generic Small Turbo-Shaft Engine Performance Data (2003) for two different Mach numbers at 10,000-ft Hd in MS Excel. The use of 10,000-ft Hd altitude in this graph was due to the fact that it is nearly the mean of the operating envelope specified in the AHS competition, 6,000 – 15,000-ft Hd, and sfc does not vary significantly with altitude within the altitude envelope the E-21 flies in. See Engine.xls.

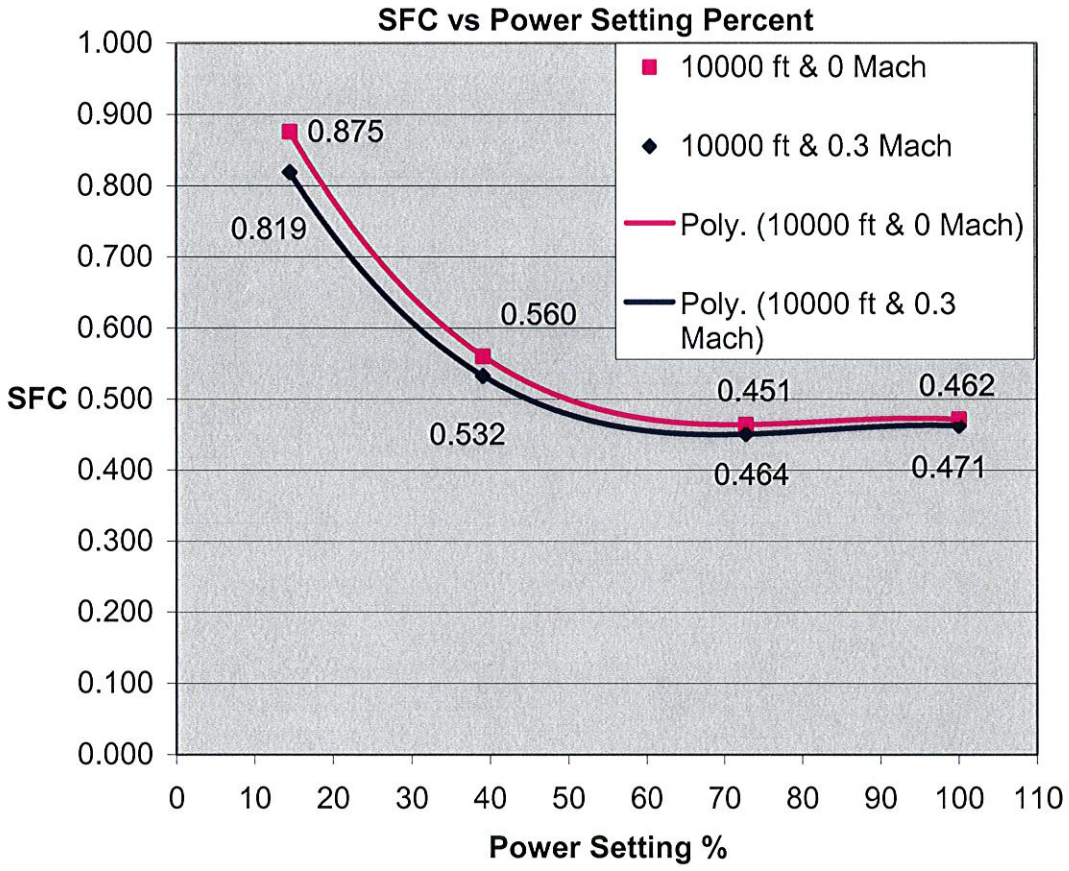

Figure 3-1 - SFC vs. Power Setting Percent

3.2.3 Fuel Consumption

Now that the sfc could be easily obtained through the use of MS Excel, finding the fuel consumption was relatively simple. The total power required for the main rotor and tail rotor was obtained for the four flight regimes: climb, cruise, hover, and descent. A similar analysis to the one in Engine paragraph 5 was performed on each flight regime to account for all power losses to obtain the total power requirement for the engines in those flight regimes. This total power requirement was then used to find a power setting and sfc. The sfc was then used to find the fuel consumptions for each different flight regime with a total fuel consumption of 1,870-lbm of Jet-A as illustrated in Table 3.2.

Table 3.2 - Fuel Consumption For Various Flight Regimes

	Time (hr)	Pr (lbf)	sfc (lbf/(hr*hp))	Fr (lbm)
Warm Up	0.033	2942.05391	0.456	45
Climb Out	0.167	1769.65453	0.451	133
Cruise Out	1.000	1128.83563	0.495	558
Hover	0.250	1435.49415	0.456	164
Cruise Back	1.000	1128.83563	0.495	558
Reserve	0.500	1128.83563	0.562	317
Descent	0.167	1072.78791	0.545	97
	3.117			1873

The main transmission is located above the cabin and directly beneath the main rotor. The main transmission reduces the engine output of 23,000-rpm by a factor of 79.52 to the 289-rpm required by the main rotor. The transmission uses 3 reductions stages for simplicity, compactness, and efficiency. The first stage is a bevel stage from the two outside engines and a spur gear stage from the center engine with a reduction factor of 2. The center engine has a spur gear reverse stage. The power is then transferred to a single large bevel gear from the three inputs with a reduction factor of 5.6. This is then reduced by a factor of 7.1 through a planetary gear. For this planetary gear system, the ring is held constant, the sun gear is the input, and the planetary gears output to the main rotor. Tail rotor power is drawn off the bottom of the single large bevel gear through a unity bevel gear stage that transmits the power to the tail rotor via a shaft that runs under the center engine. Each stage of the transmission is illustrated in Appendix C.

A power available and power required vs. speed plot could not be produced with the available data. However, because the power required curve of a helicopter is shaped like a trough with the peaks at hover and max speed, the E-21 was able to meet the power requirements for every required flight regime.

3.3 Conclusions and Recommendations

The E-21 contains three LHTEC T800-LHT-800 engines to meet the power requirement from the specification for OEI HOGE at 12,000-ft Hd capability. The ability to meet this requirement was also determined to give the E-21 the ability to meet all other power intensive flight regimes such as cruising at 145-kts at 12,000-ft Hd. The low weight, low sfc, and high power to weight ratio of the LHTEC T800-LHT-800 engines assist the E-21

in efficiently meeting the unique requirements of high altitude mountain rescue. The E-21's total fuel consumption was calculated to be 1,870-lbm of Jet-A, which is reasonable when compared to similar helicopters. The transmission design utilizes a three stage total reduction of 79.52 to combine the power from the three engines and transmit it to the main and tail rotors.

IA recommends the following four things. First, a new lightweight engine needs to be designed in the 1,000 – 1,300 shp range to take advantage of new technology and improve upon the sfc and power to weight ratio performance offered by the LHTEC T800-LHT-800. Second, design teams need to have access to detailed engine specifications including sfc and altitude performance to save time and to decrease error from extrapolating and interpolating from a rubber engine. Third, a professor with experience and knowledge in aircraft/rotorcraft transmissions will be needed to advise in future design competitions that include the preliminary design of a transmission. Fourth, a more accurate model of the main and tail rotors is required to obtain more accurate power requirements for a better estimation of the fuel consumption.

4.0 MAIN ROTOR

4.1 Geometry of the Main Rotor

The main rotor was designed to meet the performance constraints set forth by the AHS Design Competition, the most difficult being the requirement to hover out of ground effect at 12,000-ft. Hd. IA determined that if the rotor could complete this requirement with a reasonable use of horsepower, the design requirements for cruise could also be met. A conventional main rotor system was chosen, with only one rotor due to the size of the E-21 not being large enough to require two main rotors. The location of the main rotor is 5-ft above, and 0.5-ft aft of the CG. The height was determined to give the rotor blades clearance with the tail boom, and the aft location was chosen based upon Prouty's (2003) recommendations. The planform view of the E-21 main rotor is shown in Figure 4-1:

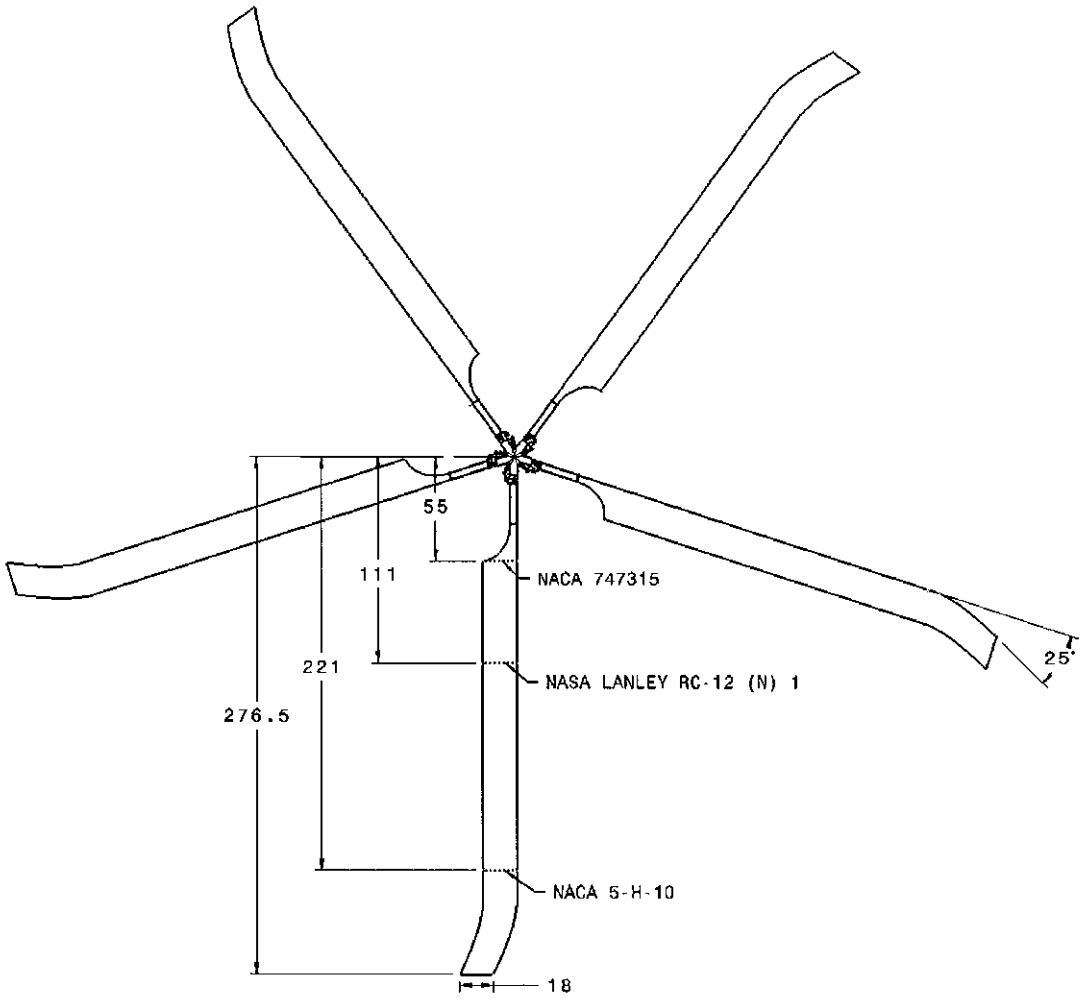

Figure 4-1 - Main Rotor Planform Drawing

The E-21 is required to hover at high altitude, therefore, blade geometries were chosen to favor these conditions. The disc loading was chosen to have a value of 6, which allows a low power required to hover, low induced velocities, and a low rate of autorotative descent (Prouty 2002). The effect of low induced velocities underneath the rotor benefits the winch operator by reducing the force felt by the blade thrust. The effect will also lessen the recirculation of snow and dust when hovering near the ground. The low disc loading lead to a chosen tip speed of 700-fps to stay above the retreating blade stall limit and below the shock limit for the cruise speed.

The main rotor system has five hingeless blades with a radius of 23-ft and a constant chord of 1.5-ft. The decision to use five blades was based upon the fact that using five blades will reduce the noise signature of the main rotor. This was considered by IA to be a selling point for the E-21 in the future, as many mountainous regions are intensifying noise restrictions. The decision to use hingeless blades was based upon the need to make the main rotor system on the E-21 a modern one. Using hingeless rotor blades causes the hinge offset to have a value of 12% instead of 5% on an articulated rotor blade. The hinge offset value drove the hub pitching stiffness moment to be larger than that of Prouty's example helicopter, even though the example helicopter is twice the weight of the E-21. The high value gives the helicopter a "snappy" response to the input of the pilot.

The blade twist was designed to be non-linear, and was custom shaped to produce the lowest horsepower required to hover at 12,000-ft Hd. Three different airfoils were chosen for their relative thickness and lift characteristics at high and low Mach numbers, and were varied along the blade length to give a more even lift distribution. By common convention, the thickest airfoil was placed inboard, and the thinnest was placed outboard. The main rotor blades have a non-linear tip sweep that is located at the last 10% of the overall blade length. The sweep was applied to the end of the blade to keep the tips from entering transonic velocities. A high blade solidity factor of 0.1 was chosen for the main rotor to keep a high chord length on the blades. A solidity factor of 0.1 will cause the main rotor blades to have a larger Reynold's number, decreasing the possibility of blade stall at high altitudes. A de-icing system was thought of for the main rotor blades, but not enough research was done to know the cost of implementing one into the design. All of the blade parameters are shown in Table 4.1:

Table 4.1 - Main Rotor Blade Parameters

Tip Speed (fps)	700	Chord (ft.)	1.5
Disc Loading (lb/ft^2)	6	Radius (ft.)	23
Blade Taper Ratio	1	Disc Area (ft.^2)	1730
Solidity	0.1	Lock Number	10.4
Blades	5	Hub-Pitching Stiffness (ft-lb)	250000
Cutout Ratio	0.2	Airfoil (0-40% of blade)	NACA 747A315
Hinge Offset	0.12	Airfoil (41-80% of blade)	NASA/LANGLEY RC-12 (N) 1
Twist (deg)	-15	Airfoil (81-100% of blade)	NACA 5-H-10

4.2 Analysis of the Main Rotor

IA performed two analyses on the main rotor system. The first analysis was done on the hover performance of the main rotor by building an Excel spreadsheet to perform Prouty's Combined Momentum and Blade Element Theory Method for estimating hover performance (Prouty 2002). The Combined Momentum and Blade Element Theory Method divides the length of the rotor blade into multiple sections and adds up the lift and drag components of all the sections to determine the thrust and torque produced by the blades. IA used 30 blade stations, instead of the minimum 10 recommended by Prouty, in order to perform a more detailed analysis of the blade performance. The analysis takes into consideration the loss of lift and torque due to the tip and the root of the blade. The hover analysis was performed at altitudes ranging from sea level to 15,000-ft Hd, to determine how the horsepower required to hover varied with altitude. The rotor power was varied by changing the collective pitch to match the estimated thrust required to hover at each altitude. This method simulated what would actually be done to hover at different altitudes.

The second analysis was done on the forward flight performance of the main rotor by using Prouty's Numerical Integration Method for estimating forward flight performance (Prouty 2002). The Numerical Integration Method was similar to the other analysis method used, except for the fact that it took into consideration the collective, flapping, and coning angles, along with the tip path plane angle of attack. The method also took into account the velocity vector acting on the blade at different inflow angles, due to the azimuth angle of the blade. IA used 30 different blade stations and 16 azimuth stations divided evenly about the disc. IA also made it possible to move the velocity vector to simulate sideslip. All of the angle inputs came from the trim spreadsheet, which used closed form equations to calculate the angles of the main rotor with the helicopter in trim at a chosen airspeed. As in the other analysis method, the rotor power was varied by changing the collective pitch of the blades, The H-force produced by the main rotor could not be calculated by the numerical integration method because of the time constraints placed on the development of the helicopter. Instead, the closed form equation for H-force was used, and did not take into consideration the affects of autorotation on the rotor system. Both analyses were limited in the fact that the airfoil data was extrapolated for different airspeeds, and the reverse flow lift and drag components were estimated for the forward flight analysis. The forward flight analysis was also found to diverge at airspeeds below 50-kts. This was due to the fact that at low airspeeds, the calculations were still accounting for the differences between the advancing and retreating sides of the disc. IA attempted to fix this by linearly phasing out this effect when the forward flight speed dropped below 20-kts. This approximation turned out to be an inaccurate model of the low speed flight regime.

4.3 Conclusions and Recommendations

IA concluded that the analysis done on the main rotor system verifies that the parameters of the main rotor produce the performance required by the AHS Design Competition. IA also concludes that the data produced by the analysis was within a reasonable degree of accuracy to continue the design of the helicopter. The analysis was capable of taking into account more factors than were outlined by Prouty, causing the analysis to be more accurate than Prouty's methods.

IA recommends that more blade stations and azimuth angles be used in the future to develop a more detailed model of the main rotor system. A more detailed analysis should also be done of the airfoils used, in reference both to the forward airspeed, and of the reverse flow characteristics. Solving for the H-force and adding the value to the trim analysis should also improve the main rotor analysis. A more accurate phase out of the velocity vector should be implemented for the analysis of forward flight at low airspeeds. More research should be done on a de-icing system for flights in cold weather.

5.0 TAIL ROTOR

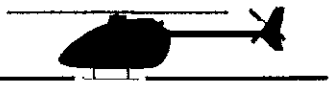

The E-21 was designed with a single main rotor. The torque force generated by the main rotor causes directional instability and must be compensated by an anti-torque device.

5.1 Configuration And Airfoil Design

There are three basic anti-torque systems used on helicopters. The first is the conventional tail rotor with a hub and blades similar to the main rotor. Second is the fenestron, or fan-in-fin system, which is basically a ducted fan in the vertical stabilizer. The third system is the NOTAR, or NO TAil Rotor, which uses engine thrust that is directed out the tail boom to counter the torque. For our high altitude hover purposes, the NOTAR would require excessive power (Stonecipher 2003). Rescue helicopter pilots interviewed expressed dissatisfaction of the NOTAR system for precision rescue flying. For these reasons, a NOTAR system was rejected for the E-21.

The rotor analysis was done by creating a spreadsheet that used Prouty's (2002) combined momentum and blade element theory method. This is the same method used for the first main rotor analysis, except due to lesser complexity of the tail blades, 15 blade stations were used. After initially iterating reasonable numbers for both conventional and fenestron configurations, it was found that a fenestron was slightly more efficient than a similar diameter conventional rotor. However, if the fenestron was designed with a small enough diameter to fit within a vertical stabilizer, it ended up requiring approximately three times the horsepower to drive than a normally sized conventional rotor. The assumptions related to the fenestron analysis were that the gains from the fenestron come from removing the tip losses. Prouty's (2002) analysis didn't provide any way to take into account the effects of the compressing of the incoming air due to the duct. The compression of the air would undoubtedly show some horsepower relief, but because the much greater requirements of the fenestron, it would still not justify the selection of a fenestron system. The other possible benefits of a fenestron system are noise reduction and safety.

After initial experimentation between fenestron and conventional, a conventional system was selected for the E-21.

Research of existing tail rotor layouts showed that the majority of tail rotor airfoils are symmetrical and that they are thicker at the root and become thinner at the tip. Since the C_{do} and $C_{l\alpha}$ data of many specialized airfoils, particularly proprietary ones used by major helicopter manufactures, are difficult to obtain, a 0012 that is tapered linearly to a 0009 airfoil was selected for the E-21. The C_{do} and $C_{l\alpha}$ data was found for the 0012 and 0009 and an average of the values was used as an estimate for the analysis.

5.2 Location and Configuration of Tail Rotor

The tail rotor placement was designed to be as high and as far aft on the vertical stabilizer as possible to minimize the disc area overlapping the vertical stabilizer. The tail rotor was mounted on the port side of the vertical stabilizer 28-ft aft and 5-ft above the CG. The tail rotor was chosen to be a pusher, that is, it blows air away from the vertical tail. The pusher design minimizes rotor-vertical tail interference. The direction of rotation was designed to be clockwise when looking at the port side of the helicopter.

5.3 Iteration

Trim analysis provided a maximum thrust that the tail must generate to balance all aerodynamic and torque forces in the worst flight regime the E-21 will encounter. The design thrust was set at 800-lb from closed form trim analysis. The design altitude was selected to be 12,000-ft because of the hover with one engine out constraint.

The combined method calculated the horsepower to produce the desired thrust. To conduct the analysis of the tail rotor, the following assumptions were made:

- Tip speed of main rotor is same as tail. This was validated by research of similar helicopters and it was found that the difference between main tip speed and tail tip speed was generally no more than ±20-ft/sec.
- Analysis is for hover. For other flight regimes, the results were considered close estimates.
- The analysis is for a generic rotor system, specifically main rotors, any error due to the smaller size of the tail rotor is not known.

The goals of the design were to minimize horsepower required while maximizing hover performance. Several iterations were conducted; the best possibilities were tabulated as shown in Table 5.1. Iteration 8 is the final design of the E-21.

Table 5.1 - Tail Rotor Iterations

Iteration	# Blades	DL	Solidity	Chord	Radius	12K TQ	12K HP	AR
-	-	Lb/Ft^2	-	Ft.	Ft.	Ft * Lb	Lb	-
1	2	20	0.2	1.0	3.6	344.4	123.6	3.6
2	2	16	0.1	0.7	4.0	365.4	117.8	5.5
3	3	20	0.2	0.7	3.6	387.4	139.9	5.4
4	3	25	0.2	0.6	3.2	381.0	154.0	5.3
5	4	16	0.1	0.4	4.0	403.9	130.9	10.2
6	4	16	0.3	1.0	4.0	411.1	132.4	4.1
7	4	20	0.3	0.9	3.6	400.0	144.0	4.1
8	**4**	**16**	**0.2**	**0.7**	**4.0**	**416.7**	**133.6**	**5.5**
9	4	30	0.4	1.0	2.9	386.0	170.0	3.1
10	4	20	0.4	1.2	3.5	405.0	145.0	3.0
11	4	16	0.4	1.3	4.0	421.0	135.0	3.1
12	4	30	0.3	0.6	3.0	391.0	173.0	5.0
13	4	20	0.3	0.7	3.6	397.0	143.0	5.1
14	5	16	0.2	0.5	4.0	406.3	131.4	7.7

5.3.1 Sizing

For sizing consideration, Prouty (2002) developed an equation from historical data shown in Figure 5-1:

$$D_T = \frac{D_M}{7.15 - 0.27 D.L._M}$$

Figure 5-1- Curve fit of historical data for tail rotor sizing.

The equation in Figure 5-1 yielded an estimated tail rotor diameter of 8.3-ft. This number was used as a general target for the tail rotor size.

Initially, iteration 12 was pursued because a 6-ft radius would keep the tail rotor out of they way for rear door entry. After the vertical tail was sized, it became apparent that the tail would blank too much of the tail rotor. The design was modified to iteration 8, that has an 8-ft diameter and is also is closer to Prouty's sizing equation result. Placing the tail rotor higher on the vertical stabilizer and adding a stinger to guard against coming in contact with the rotor solved the rear door access safety issue. The diameter of the E-21 tail rotor was finalized at 8-ft.

When choosing the number of blades, the minimum was chosen as four because of noise consideration. Prouty (2002), gives a rule-of-thumb for the blade aspect ratio to be between 5 and 9. The E-21 has four tail rotor blades with an aspect ratio of 5.6.

5.3.2 Blade Design

Twist for the tail rotor was initially chosen to be –8°. The final twist was chosen to be -2°. Though the higher twist of -8° does have slightly higher hover performance, the -2° twist was chosen because of trim considerations. The change to -2° twist caused a very small reduction in hover performance but this loss is offset by an increase in vortex ring state resistance (Prouty 2002). The lessened twist also increased horsepower required by about 5-hp.

5.4 Final Design Parameters

Table 5.2 shows the final design parameters of the E-21 tail rotor. Figure 5-2 shows a drawing of the tail rotor. A detailed planform drawing of the tail can be found in Appendix C.

Table 5.2 - Tail Rotor Final Design

Tip Speed (fps)	700	Chord (ft.)	0.7
Disc Loading (lb/ft^2)	16	Radius (ft.)	4
Blade Taper Ratio	1	Disc Area (ft.^2)	52
Solidity	0.2	Lock Number	2.7
Blades	4	Hub-Pitching Stiffness (ft-lb)	4200
Cutout Ratio	0.4	Sea Level HP Required (hp)	113
Hinge Offset	0.06	12,000 ft. HP Required (hp)	130
Twist (deg)	-2	15,000 ft. HP Required (hp)	136

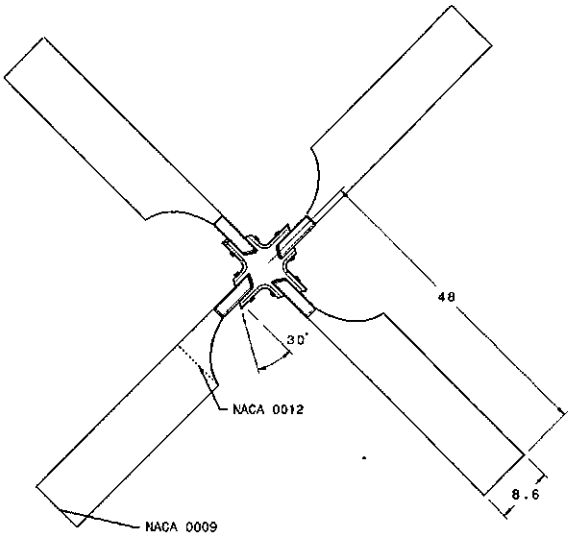

Figure 5-2 - Tail Rotor

5.5 Analysis of Final Design

After the sizing was completed, the analysis could be modified so that the sizing parameters remain constant and the horsepower for any thrust can be computed. The thrust required for different flight regimes came from the closed form trim analysis. When the horsepower for the desired regimes were calculated, they were used for propulsion system analysis.

5.6 Tail Rotor Design Conclusions

The final design of the tail rotor presents characteristics that fulfill the design goals of maximum performance for minimal horsepower required. The sizing that the combined blade element and momentum equations determined is consistent with similar helicopters, which provides confidence in the calculated numbers of our spreadsheet.

A problem was discovered when trying to find the power required for small thrusts. If the thrust drops below 200-lb or if negative collective is required, the equations no longer work. This issue with the analysis causes problems when calculating horsepower for decent and high altitude sideslip with crosswind.

For future work, a new and specialized analysis designed for the unique characteristics of a tail rotor needs to be developed. The characteristics that need to be taken into account are the possibility of negative collective, azimuth sweep for flapping, and hub angle with pitch-flap coupling. Finally, a de-icing system for the tail rotor is planned to fulfill recommendations put forth in the AHS design competition.

6.0 LANDING GEAR

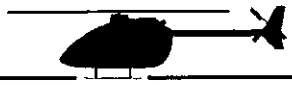

Tubular skids were chosen as the landing gear for the E-21. On large helicopters, choosing wheels may be an advantage, however, wheels also tend to weigh much more than skids. Moving large helicopters can be challenging task to move on the ground without wheels. IA took this consideration when designing the E-21, but decided that the helicopter was not large enough to make wheels a necessity. IA decided upon a skid landing gear system because a skid system would save weight and money. Also, skids are much less complex and a helicopter the option to land in snow with the addition of snowshoes as well as a sloped surface. The driving factors when choosing the landing gear were weight and ability to land in snow, therefore, skids were found to be the best choice.

No specific tip-over or ground clearance requirements were found. Therefore, IA set a goal of having the E-21 being capable of landing on a slope of six-degrees. In order to determine whether or not the E-21could meet this personal standard, a static tip-over analysis was done on the landing gear. This process involved summing the moments about one of the skids to determine the degree of slope that would cause the helicopter to tip over. The results concluded that the current landing gear configuration allowed the E-21 to sit on a slope up to 33-degrees and flare at an angle of ten-degrees. However, IA later calculated that his method only showed that the E-21 could only rest at this slope angle and not actually land on it. The final analysis determined that the helicopter is unable to land on a slope greater than two-degrees of left slope and less than four-degrees of right slope.

There also was an initial concern about the clearance between the wench cable and the landing skid. As the winch pulled a victim up, there was a very small margin of clearance between the skid and the cable. This problem was resolved by increasing the arm of the existing winch so that there was greater clearance between the skid and the cable. The dimensions of the landing gear are 112-in wide by 120-in long and 22-in high. For further details, see the final three-view drawings in section 10.

IA chose the skid landing gear system because of the reduction in weight as well as the fact that it offered the E-21 the capability to land in a sloped environment. However, future analysis will be done in the area of ground clearance requirements and tip-over criteria. IA recommends that more research be done in this specific area to verify the current analysis of tip-over.

7.0 WEIGHT AND BALANCE ANALYSIS

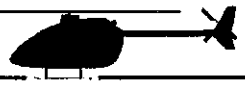

7.1 Preliminary Structural Arrangement

IA designed the E-21's structural arrangement differently than Roskam's method of fixed-wing airplane design. IA designed the side and rear doors to accommodate the needs of a rescue helicopter crew.

Knowing the placement of doors allowed IA to focus its primary efforts on the placement of the rotor systems. Following historical trends, the power plants were placed on top of the fuselage structure along with their supporting systems (generators, rotor hub, hydraulics, and environmental controls). The helicopter's fuel tanks were initially placed on the top portion of the fuselage but were later moved down into the belly of the helicopter during the Class II weight and balance calculations. This was done to alleviate the required structure of the bulkheads.

7.2 Weight and Balance Calculation

IA used Prouty's preliminary weight estimation method to conduct its Class II weight and balance analysis. Prouty's equations broke down the helicopter's individual systems such as the drive, electrical, controls, fuel, and environmental systems. Each weight was determined by using specified inputs listed in Prouty's (2002) equations. Table 14.5 lists the calculated results of the individual weight components.

The center of gravity was calculated by first establishing a datum for the x (fuselage station), y (butt line), and z (water line) directions. Next, a positive coordinate system was created and each component within the helicopter was assigned a location (Appendix C). Once all the components and their weights were listed, the helicopter's center of gravity was calculated (Appendix B, Table 18.1 through 18.4). IA simulated various weight and balance layout by placing certain items in their most extreme position to produce the worst possible center of gravity. IA then performed a trim analysis with the different CG layouts to determine if the E-21 was stable. Table 7.1 shows the CG positions for various flight regimes as well as how the vertical CG traveled as fuel was consumed.

Table 7.1 - CG Location For Various Flight Regimes

	x (ft)	y (ft)	z (ft)
EMPTY	9.7337	0.0282	5.7800
MAX GROSS	9.6219	0.0184	4.0461
IN-FLIGHT	9.6219	0.0184	4.0461
HOVER	9.5852	0.3701	2.8222

7.3 Analysis of Weight and Balance Results

Compared to the Class I estimate of 10,000-lbs, Prouty's (2002) Class II weight and balance calculations produced a max gross weight of approximately 9,500-lbs. Though the CG traveled no more than four inches in both the x and y directions, the CG traveled over three feet vertically (see Figure 7-2) as opposed to four feet from the Class I analysis. Also, the CG analysis showed that the E-21 was not dependent upon a specific loading method (front to rear or vice versa) which is shown in Figure 7-1.

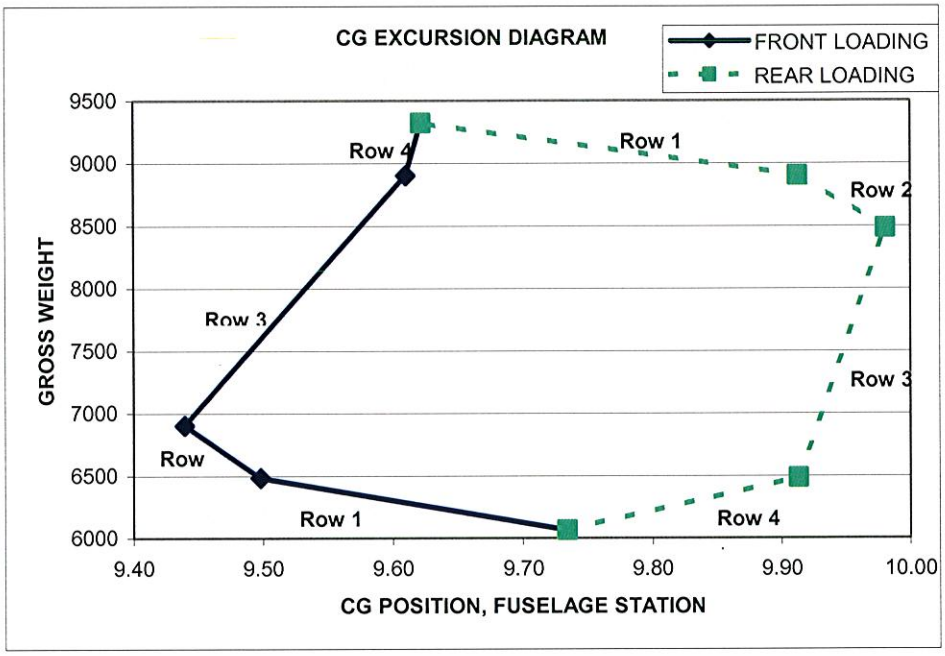

Figure 7-1 - CG Excursion Diagram

This travel is largely due to the fact that the crew, passengers, and fuel, are located relatively close to the floor of the cabin, thus lowering the CG significantly in flight. Table 7.2 lists the vertical CG as fuel is consumed from the max gross configuration.

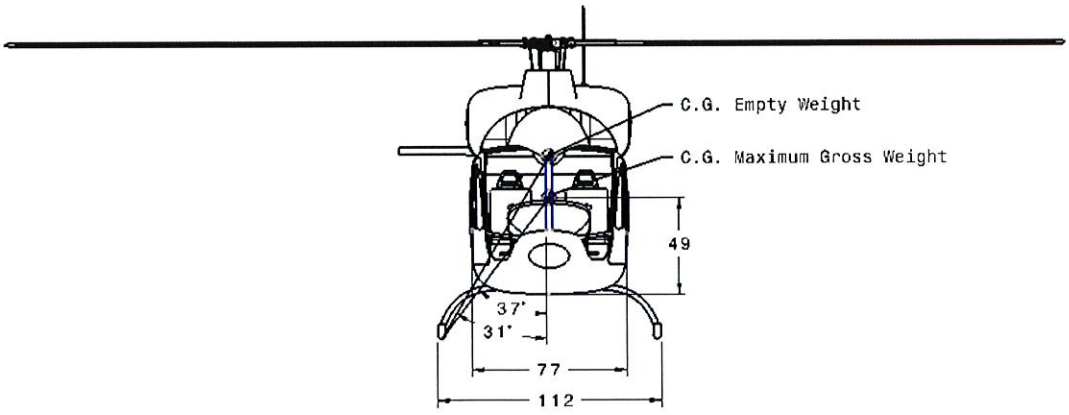

Figure 7-2 - Vertical CG Travel

Table 7.2 – CG Travel In Flight

Fuel (lbs)	z (ft)	Weight (lbs)	z-moment (ft-lbs)
2000	4.0461	9321.5	37715.7
1800	4.1239	9121.5	37615.7
1600	4.2051	8921.5	37515.7
1400	4.2901	8721.5	37415.7
1200	4.3790	8521.5	37315.7
1000	4.4722	8321.5	37215.7
800	4.5701	8121.5	37115.7
600	4.6728	7921.5	37015.7
400	4.7809	7721.5	36915.7
200	4.8947	7521.5	36815.7
0	5.0148	7321.5	36715.7

7.4 Conclusions and Recommendations

IA achieved its goal of minimizing the CG travel by specifically placing various components throughout the helicopter to offset each other. By arbitrarily selecting an approximate CG (primarily for the placement of the main rotor), IA was able to appropriately place the larger items such as engines, generators and fuel tanks close to the CG thus minimizing the CG travel in all flight regimes. These equations specifically asked for information such as the number of rotor blades required, polar moment of inertia and tail rotor criteria which in turn produced the various component weights needed to conduct the Class II weight calculations.

Prouty's method for the Class II weight and balance analysis was more appropriate than Roskam's because Prouty's method specifically dealt with the preliminary design of helicopters and provided better equations used in the weight calculations.

IA also recommends that a more detailed analysis of other weight components such as the weights of the engine cowlings, fuselage structure, and both the horizontal and vertical stabilizers be conducted. This will allow for a better estimation of the overall weight of the helicopter and will help refine the current CG location throughout all flight regimes. Although the Class II weight and balance analysis produced a gross weight of approximately 9,500-lbs, IA believes that the E-21 will weigh closer to 10,000-lbs (the max gross weight of the original weight estimate). This is primarily due to the fact that more research will be done in the future and that the manufacturing process will most likely add weight to the overall design of the E-21 HAMR.

Another area that IA would like to investigate is the ergonomics of the various components within the helicopter such as the rescue hoist, and medical equipment. IA would like to determine whether the current placement of these components will help or hinder the crew's capabilities during rescue operations.

8.0 STABILITY AND TRIM ANALYSIS

8.1 Theory

The stability and control analysis only took into account the static trim of the aircraft. If the aircraft could be statically trimmed, it was assumed to fly in that regime. The analysis only covered the most sensitive flight regimes dictated by the mission profile, the most difficult regimes being the OEI HOGE 12,000-ft Hd and HOGE 15,000-ft Hd, both with 40-kts of crosswind. The aircraft analysis was designed to handle both sideslip and angle of attacks from +90 to –90 degrees. The helicopter was modeled with six degrees of freedom, which followed Prouty's (2002) methods. The axis was fixed to the body following a right-hand coordinate system with the positive x-axis out the nose. The trim limits of the aircraft were set by looking at the desirable cyclic and collective movements picked from ranges based on historical data from Prouty's (2002) text. If the aircraft could be trimmed with these constraints on the amount of cyclic and collective input, the aircraft could theoretically fly in that regime. In addition to the evaluation of cyclic and collective positions trends of movement were also analyzed. The more forward cyclic added, the faster the helicopter will move foward. The low airspeed longitudinal cyclic position was another point of interest for the trim analysis. Ideally, there should be a neutral to slightly forward stick position in hover to low forward flight regimes. Also, there should not be an aft stick position to trim in this regime. Cyclic and collective stick positions and trends will be discussed later. A slope-landing regime was modeled to help determine the slope landing capability along with the tip-over limits. The slope landing was modeled by adding a force and a moment into the governing trim equations. The maximum slope-landing angles were found by iterating the skid forces from zero to gross weight.

The forces and moments accounted for in the aircraft trim equations only included contributions from the fuselage, main rotor, tail rotor, and tail empennage. The fuselage contributed weight, three-dimensional drag polar forces, a pitching moment, and a yawing moment. The main rotor forces and moments accounted for were thrust, hub-pitching stiffness, drag in the x-direction, and torque. Thrust was the only force the tail rotor contributed to the trim equations. The tail empennage was broken down into vertical and horizontal surfaces that contributed both lift and drag forces.

8.2 Design

The trim equations were used to integrate all of the aircraft's components and check the feasibility of the design layout to see if the E-21 will fly. Trim equations were also used to size the tail empennage. The horizontal tail was designed with a download (+ z-direction), and was moved forward or aft to help shift the longitudinal trim points to best meet all the different flight regimes. If the body was pitched down more than desired, the horizontal tail was shifted aft and area was increased to give the optimum lift through all forward flight speeds. The horizontal tail design trade-off was if the area was made too big, it would become detrimental to the hover performance by increasing the drag. The

incidence could also be changed to give the most desirable lift and drag characteristics in all analyzed flight regimes. Changing the incidence also helped solve the problem of reaching large horizontal tail areas. The horizontal tail's center of pressure had a positive y offset. This design helped counter the aircraft's tendency to roll to the left due to the moment generated by the main rotor when the advancing blade flaps up. The effect was not significant but did help and also made it possible for room to place the tail rotor at the best possible vertical location with respect to the aircraft's CG.

The vertical tail was handled similarly to the horizontal tail. The vertical tail was shifted aft to add better weathercock stability when in a crosswind. Increasing the area also helped but added more drag. The incidence of the vertical tail was adjusted to help reduce the tail rotor thrust needed. The greatest benefit was seen in forward flight at high airspeeds, in which the incidence angle gave the surface more angle of attack for more lift, thus reducing the thrust needed by the tail rotor. The center of pressure of the vertical tail (z- direction) was kept as close as possible to the aircraft's center of gravity to minimize the rolling moment. The tail rotor was placed on the downwind side of the vertical tail so the downwash would not impinge upon the vertical stabilizer making for a less draggier design. The lift and drag on the vertical and horizontal surfaces took in account lift and induced drag on an airfoil phased out over an increasing sideslip angle with the addition of drag on a flat plate phased in over the sideslip angle. Table 8.1 shows the geometries of both the horizontal and vertical tails.

Table 8.1 - Tail Geometries

Geometry	Horizontal Tail	Vertical Tail
Area (ft^2)	18	20
Airfoil	NACA 0012	NACA 0012
CP from CG x (ft)	28	28
CP from CG y (ft)	2	-
CP from CG z (ft)	-	3
Incidence (deg)	-3 (leading edge down)	4 (leading edge to the right)
AR	2.17	2.87

The trim analysis based the geometry off of the aircraft's CG. A very thorough layout of weight and balance analysis was performed to minimize the CG travel. IA concluded that the longitudinal and lateral directions moved insignificantly warranting no need to recalculate aircraft trim. The vertical CG traveled roughly three feet upwards due to fuel burn and different aircraft loadings; a complete analysis of how the aircraft trim was affected was not performed by the time of this paper.

The following figures show the longitudinal and lateral trim angles.

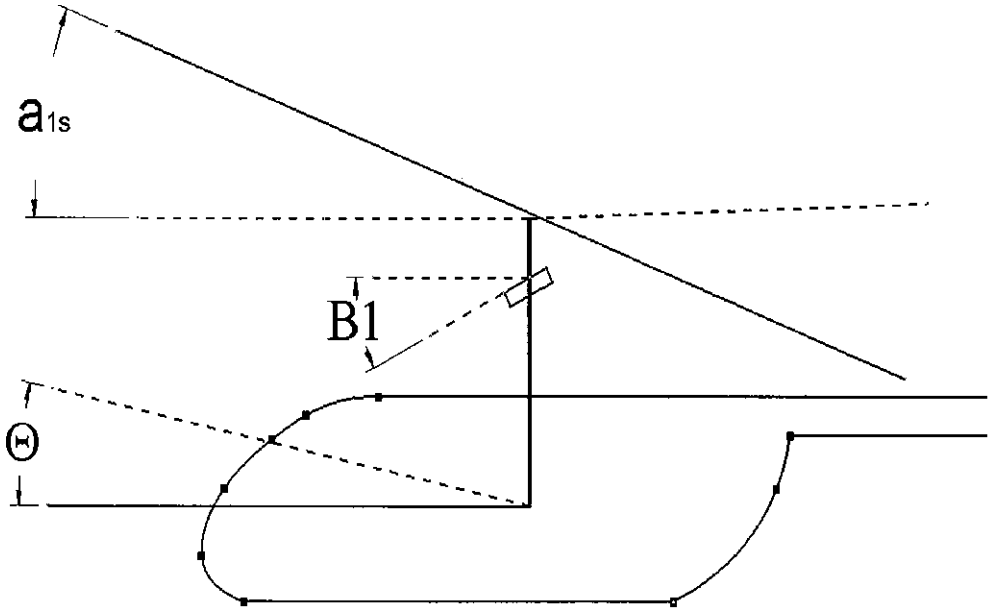

Figure 8-1 – Longitudinal Trim Angles

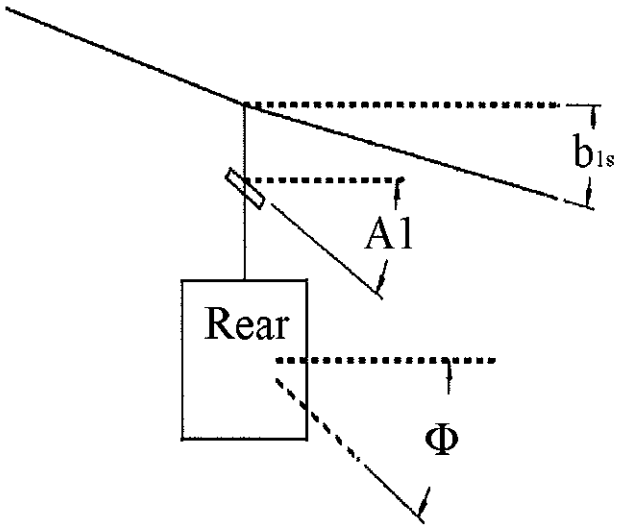

Figure 8-2 - Lateral Trim Angles

The following two figures show the cyclic and collective positions and trends as functions of airspeed.

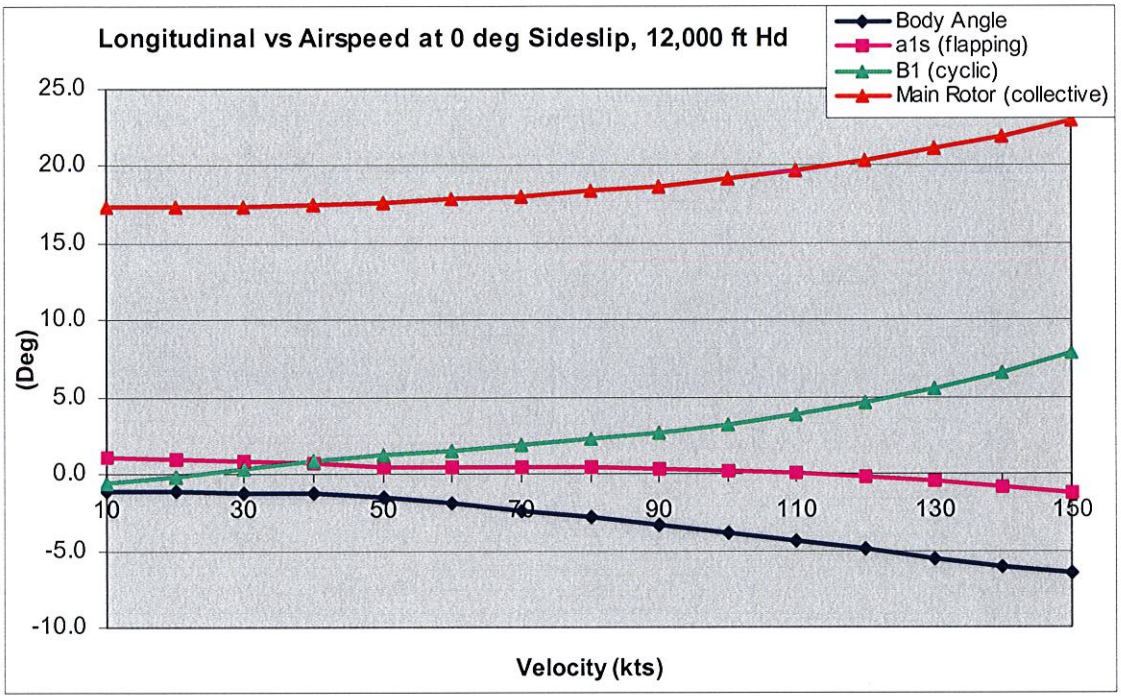

Figure 8-3 - Longitudinal Trim vs. Airspeed

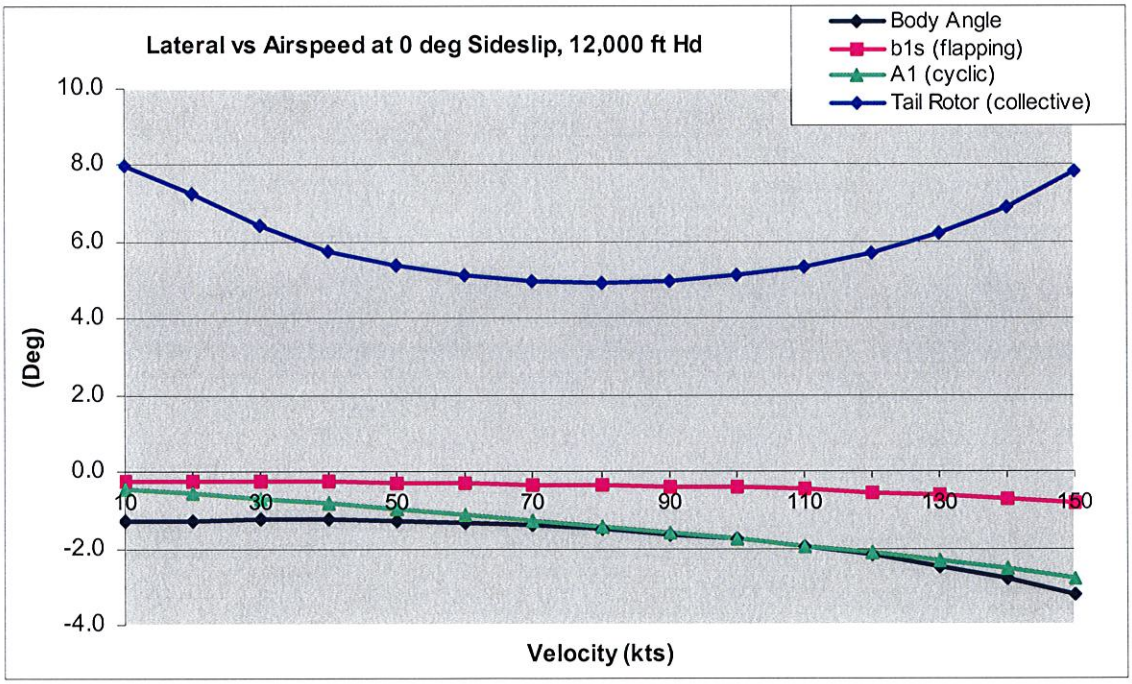

Figure 8-4 - Lateral Trim vs. Airspeed

Figure 8-3 shows the longitudinal trim points as a function of forward airspeed. The longitudinal cyclic position is still undesired being at a negative cyclic position while moving forward at 10-kts. This means that the pilot has to hold negative cyclic to maintain a 10-kt forward airspeed. This problem may be fixed through control rigging. However, the cyclic trend is desirable showing more use of forward cyclic as airspeed increases (push forward to go faster).

Figure 8-4 shows the body roll angle needed to achieve trim in forward flight; the left body roll angle is a combination of: the main rotor thrust offset caused by the advancing blade flapping up, the positive y thrust of the tail rotor, and the lift on the vertical tail at higher airspeeds.

The following two figures show the cyclic and collective positions and trends as a function of sideslip.

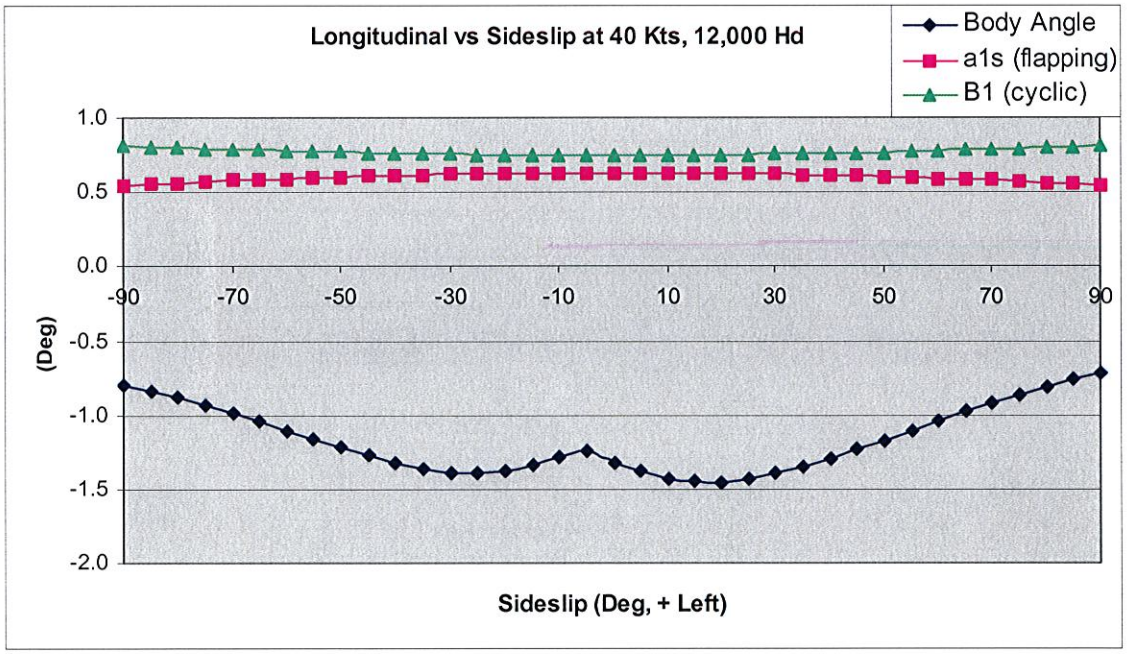

Figure 8-5 - Longitudinal Trim vs. Sideslip

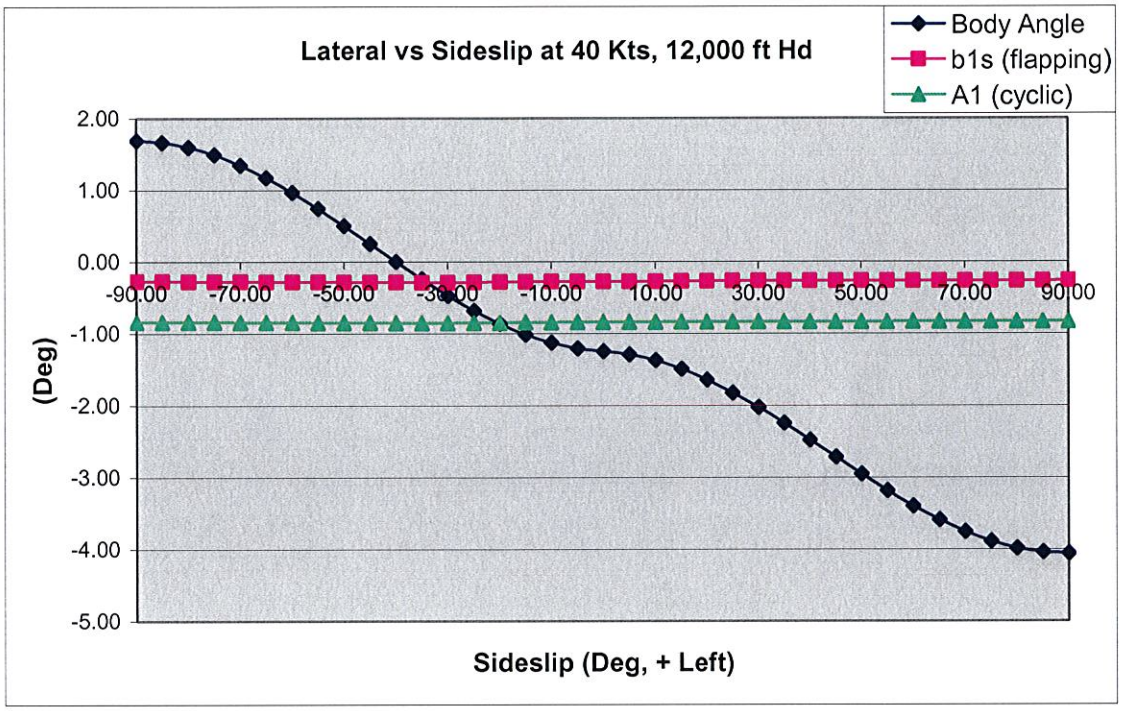

Figure 8-6 - Lateral Trim vs. Sideslip

In Figure 8-5 the decrease in body down pitch angle at zero degree sideslip is caused by the lift gained on the horizontal tail. The most lift on the horizontal tail is seen at 0-degrees sideslip and then phased out over sideslip as a function of cosine. The trend of needing slightly more aft cyclic in 0-degrees sideslip then in 90-degrees is not desirable. This can be explained by the nose down pitching moment on the fuselage caused by the longitudinal drag on the fuselage, as the fuselage pitches down aft cyclic is needed to trim the aircraft. The decrease in body angle at 0-degrees sideslip is caused by the increased lift on the horizontal tail that overcomes the nose down pitching moment caused by the drag on the fuselage. This shows that the analysis of phasing drag and lift as functions of sine and cosine cannot be a realistic approximation.

The lateral trim, in Figure 8-6, shows intuitive body angles; with a 90-degree sideslip from the right side, the aircraft rolls into the sideslip. As the body rolls into the sideslip no more lateral cyclic is needed due to the fact that the main rotor shaft is also rolled into the sideslip pointing the general thrust vector into the wind. This is why the lateral cyclic and flapping angles remain close to constant.

8.3 Trim Conclusions And Recommendations

Some of the difficulties encountered or found during the trim analysis include the designing of a tail rotor and vertical tail capable of handling the high torque of the main rotor. The tail rotor thrust needed was positive for every position along the 40-kt sideslip sweep from +90 to –90 degrees. In a 40-kt direct left crosswind the pilot would still have to use left pedal to overcome the main rotor torque, which was higher than the weathercock force on the 20-ft^2 vertical tail at a moment arm of 28-ft. The pilot uses left pedal or positive thrust regardless the direction of the crosswind. It was concluded that it seemed excessive to only use left pedal in a direct left crosswind and would be undesirable from a pilot's perspective. Historical data shows the range of tail rotor collectives average from –10 to 20-degrees (Prouty 2002). The tail rotor collective used in the trim analysis was from –4 to 16-degrees, which shows that the aircraft is more on the positive end of the collective range and may have problems commanding left yawing rates in a 40-kt crosswind from the right. IA tried resizing the vertical tail for better weathercock stability, and found that an area of 40-ft^2 would have been needed. This worked in the hover regime but at high airspeeds the closed loop tail rotor calculation broke the low collective limit of –10 degrees having to produce very high negative thrusts. The team would like to further investigate this tail rotor problem.

The analysis also did not take in account autorotation. The main rotor was designed to yield thrust for powered flight and at certain airspeeds and descent angles the analysis yielded negative torque. When the aircraft yielded a negative torque it was said to be in autorotation and no correct aircraft geometry was available. Negative torque indicated that the rotor was doing work on the engine from an inflow up through the rotor system. Future work needs to be done developing this part of the analysis.

Another difficulty was the main rotor's hub-pitching stiffness at 250,000-ft-lb, due to the choice of a hinge-less rotor hub, making it very difficult to perform slope landings. The max slope landing that the aircraft could do was less than 2-degrees for a left slope and lees than 4-degrees for a right slope. This is not desirable; the team would like the aircraft to land on at least 6-degree slopes. The solution to this problem would be to go with a fully articulated rotor hub, but the benefit to having a high hub-pitching stiffness is that the aircraft will be more maneuverable as moments are transferred faster back and forth between the rotor system and the body, making for less lag time between control inputs and results. The flapping angles of the main rotor system were very small due to the fact that the analysis only took in account the aircraft in static states and a high hub-pitching stiffness. The flapping angle limits, which are needed to know the amount of clearance underneath the rotor system, can only be seen in transient states, which this analysis did not cover.

The main rotor drag was only calculated in a closed loop solution. Building a numerical solution that matches the existing main rotor solution may yield better results.

The limit encountered with the tail rotor numerical integration solution was that the analysis could not calculate negative collectives for low positive tail rotor thrusts. The

closed loop solution was used in the trim equations with the numerical integration solution used for optimizing the geometry and calculating the horsepower needed.

No analysis was performed on how the horizontal tail surface was affected by the main rotor downwash based on its radial location underneath the main rotor system due to the fact that the main rotor downwash was too difficult to predict. The aircraft could have been trimmed more precisely in hover if this was known.

IA also looked into the concept of an asymmetrical shaped tail boom to help relieve the tail rotor of some of the thrust needed during hover. No analysis was performed due to the need for wind tunnel test data and not enough known about the main rotor wake. Further work is needed in this area for a complete analysis.

The trim analysis yielded that the aircraft met the requirement for the 40-kt crosswind from any azimuth while OEI HOGE at 12,000-ft Hd. The Aircraft was able to also have a cruise speed of 145-kts, which was not as hard to meet based on this analysis. The analysis also showed that IA met the 40-kt crosswind from any azimuth while HOGE at 15,000-ft Hd. Other regimes requiring less power were not examined as thoroughly due to time constraints.

9.0 DRAG ANALYSIS

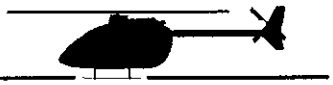

9.1 Forward Flight

The Drag on the fuselage was calculated from three directions: Vertical or Z direction, Forward or X direction, and Side or Y direction. Drag due to the velocity of the helicopter moving through the air was calculated by splitting the fuselage into different sections along the fuselage. The area of each section was calculated from the top and side views. These sections were each assigned a drag coefficient according to their shape. Multiplying the drag coefficient of drag and the corresponding area and the dynamic pressure gave a force. These forces were added up for each section along the fuselage to get the total drag for either vertical or side force. The forward drag was calculated by assigning a drag coefficient to each part of the fuselage; engine nacelles, skids, FLIR, etc. The forward drag force was calculated by multiplying the areas, by the coefficient of drag, by the dynamic pressure.

9.2 Main Rotor Induced

Drag induced by the main rotor over the fuselage was calculated by breaking up the fuselage and tail boom into projected areas using the same blade station locations as in the main rotor analysis. The induced velocities from the main rotor vary as a function of blade radius. The exact dynamic pressures (q) from each station were taken from the main rotor analysis during hover and a correction factor of 3.3 was used to curve fit the data to induced q graphs from Prouty (2002). From these dynamic pressures, drag over each station on the fuselage was calculated by multiplying the dynamic pressure, estimated C_d from generic shapes, and projected area. All the individual drag forces were summed, yielding a total drag due to the main rotor.

9.3 Total Vertical

The total vertical drag was calculated by adding the drag due to the rotor with the drag due to vertical flight. If the helicopter is descending the drag due to vertical flight is negative and therefore subtracts from the drag due to the rotor wash. In addition, it was assumed that if the helicopter were moving forward at 20 knots the rotor wash would be pushed aft of the fuselage. The calculation of vertical drag phased the rotor wash out linearly as the forward speed increased. The same linear phasing was done as the side velocity of the helicopter increased.

9.4 Total Drag Force

The drag forces were combined for any given angle of attack and any given sideslip. This was done by assuming the velocity vector could be broken into components in each of the three drag directions. With the components of velocity in each direction the drag force could be calculated in each direction.

Fuselage pitching and yawing moments were calculated by historical data and were gross estimations. A fuselage shape similar to the E-21 was analyzed in Stability and Control

of Helicopters (Prouty, 2002), the fuselage coefficient of pitching moment was picked at various angles of attack according to this data. A graph of the pitching moment coefficient versus angle of attack is shown in Figure 9-1.

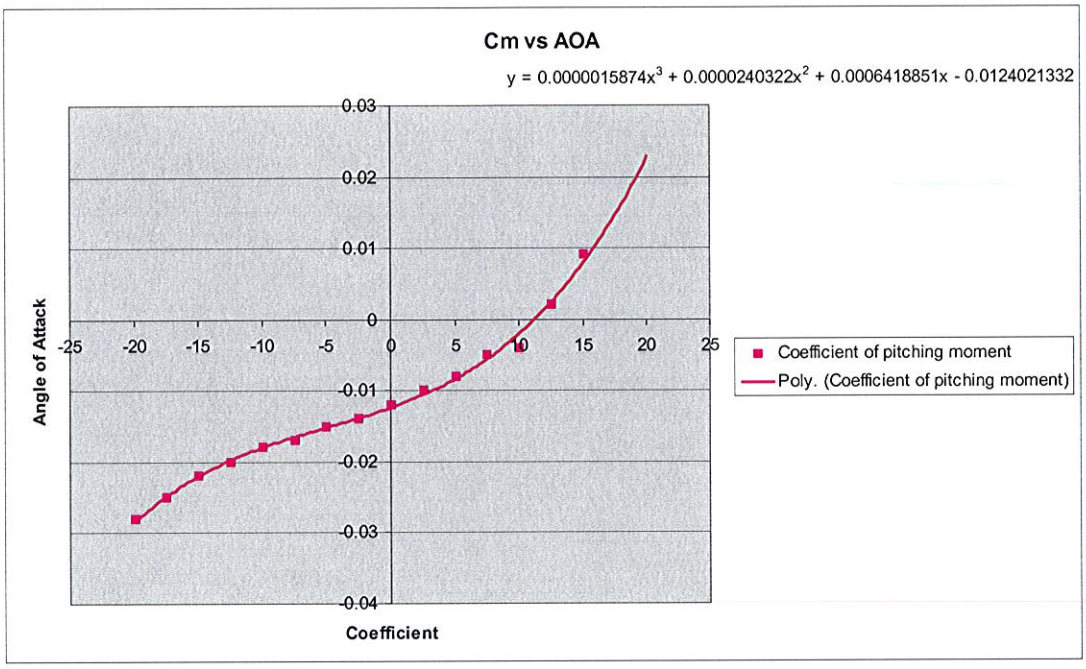

Figure 9-1 - Cm vs AOA

The yawing moment coefficient was assumed to be constant for various angles of sideslip and it was determined to be destabilizing because of the large area that is in front of the center of gravity. The coefficient was picked from historical data and was slightly adjusted to yield expected data.

9.5 Conclusions and Recommendations

The drag analysis performed followed Prouty's (2002) methods applied to three-dimensions, which included breaking up the fuselage into common shapes with known drag coefficients and extrapolating moment coefficients from Prouty's wind tunnel data. The shapes were gross estimates in conjunction with the three-dimensional application and IA believes that a better drag analysis could be performed with wind tunnel testing.

10.0 FINAL THREE-VIEW

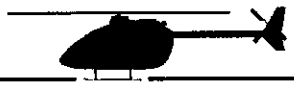

The following page shows the 3-View of the E-21.

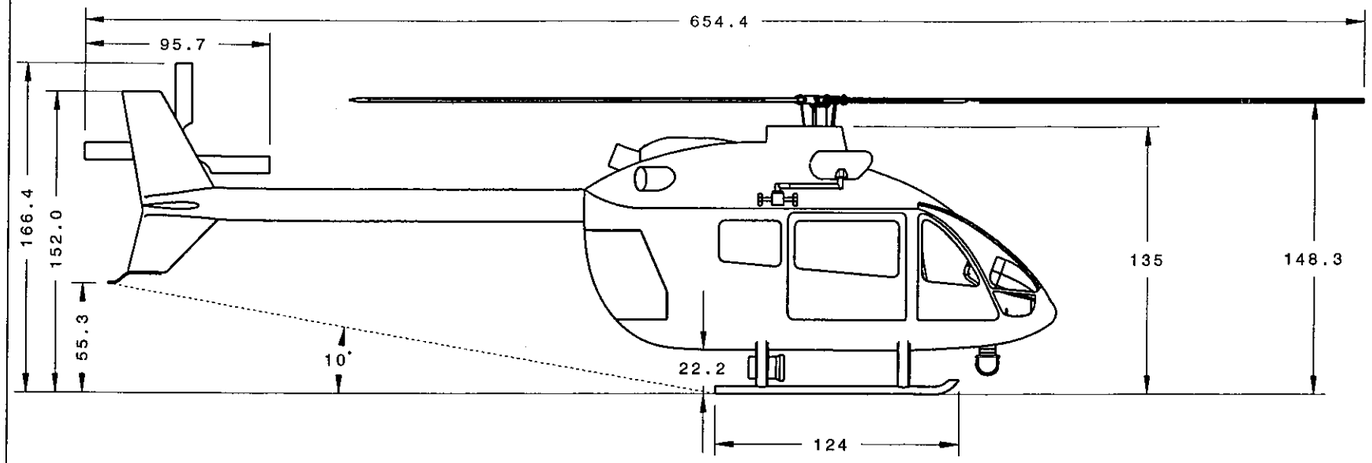

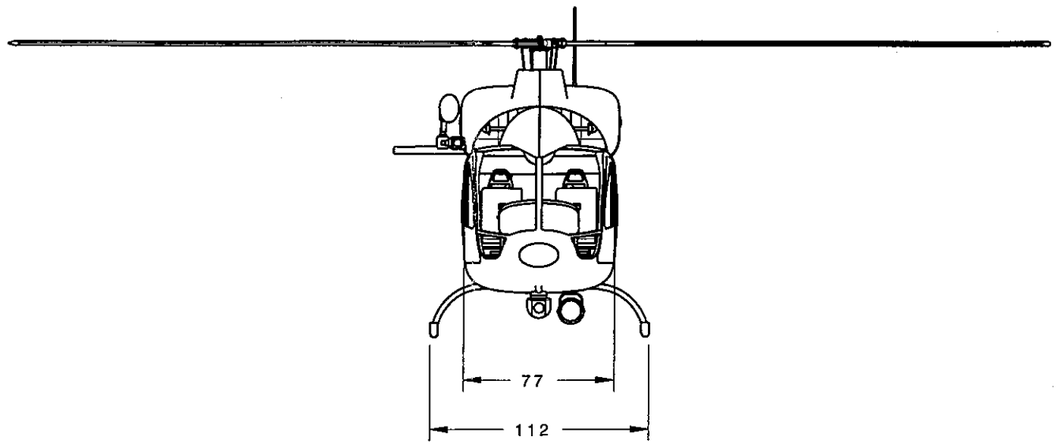

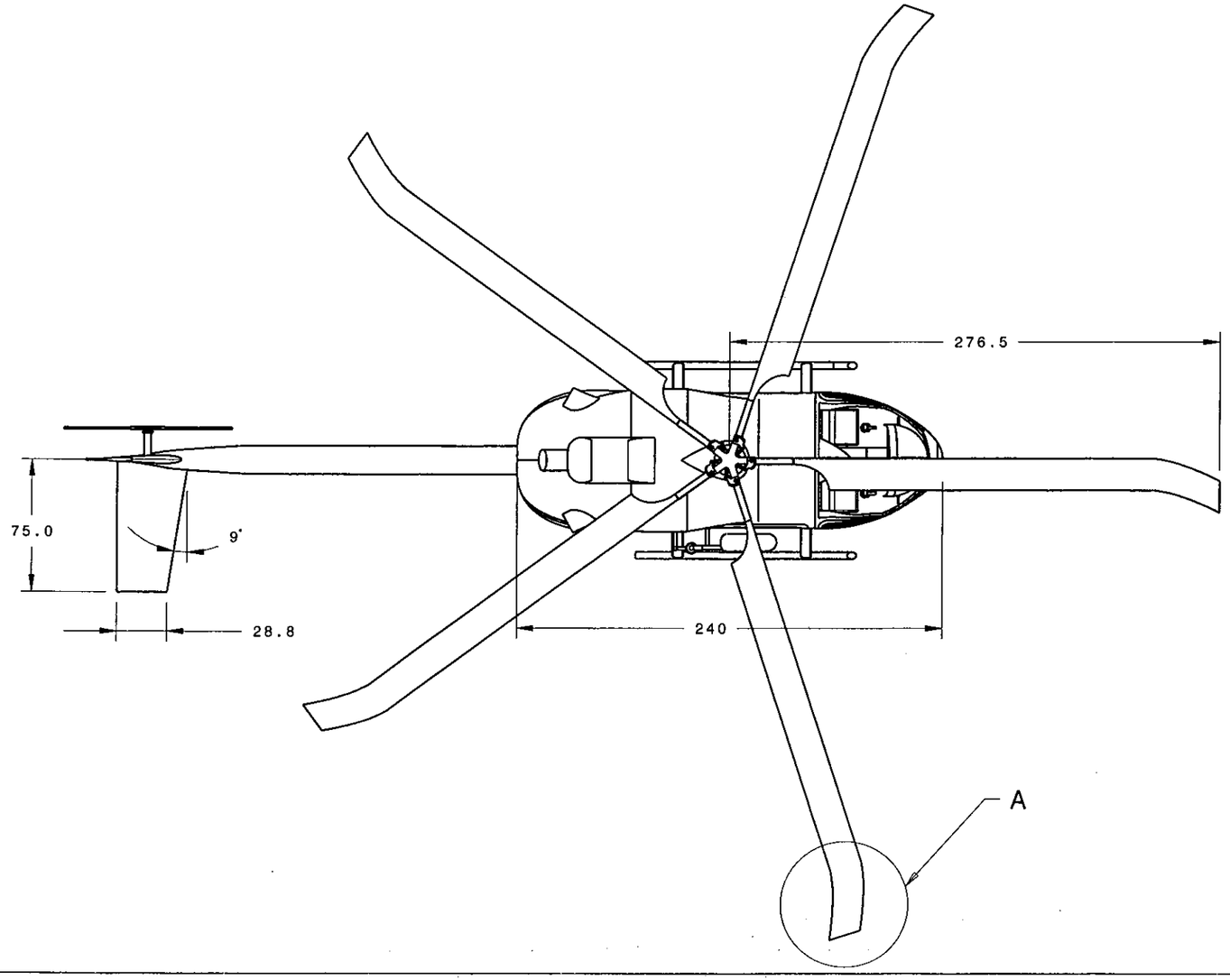

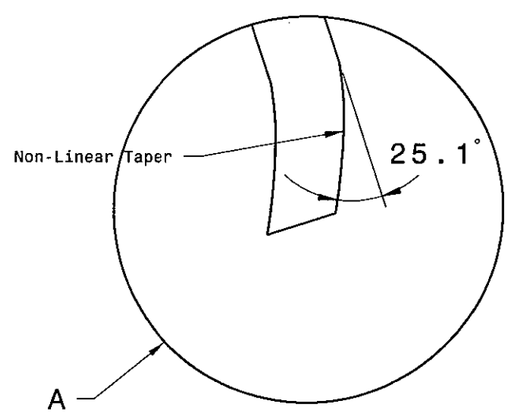

Infinity Aerospace
Embry-Riddle Aeronautical University
3700 Willow Creek Rd.
Prescott, AZ 86301
Aerospace Engineering Dept.

Drawing Discription:

Three View Drawing of the E-21 HAMR

SIZE	CODE IDENT NO.	8:1 DRAWING NUMBER:	OF	REVISION
B		DIMENSIONS	INCHES	A
		DRAWN BY:	BRET DAVENPORT	
SCALE 1 : 75		SPEC:	SHEET:	OF

11.0 CONCLUSIONS, RECOMMENDATIONS & MISSION VERIFICATION

The conventional helicopter configuration was chosen because it best fits the needs of IA's search and rescue mission. The cabin was laid out due to the ergonomics of the mission of loading of and tending to the patients. The fuselage was derived by finding the best and most practical places for all the equipment and other parts.

The E-21 contains three LHTEC T800-LHT-800 engines to meet the power requirement from the specification for OEI HOGE at 12,000-ft Hd capability. The ability to meet this requirement was also determined to give the E-21 the ability to meet all other power intensive flight regimes such as cruising at 145-kts at 12,000-ft Hd. The low weight, low sfc, and high power to weight ratio of the LHTEC T800-LHT-800 engines assist the E-21 in efficiently meeting the unique requirements of high altitude mountain rescue. The E-21's total fuel consumption was calculated to be 1,870-lbm of Jet-A, which is reasonable when compared to similar helicopters. The transmission design utilizes a three stage total reduction of 79.52 to combine the power from the three engines and transmit it to the main and tail rotors.

The main rotor analysis followed Prouty's design methods and produced rotor geometries that satisfied the AHS performance requirements. IA recommends that more blade stations and azimuth angles be used in the future to develop a more detailed model of the main rotor system. A more detailed analysis should also be done of the airfoils used, in reference both to the forward airspeed, and of the reverse flow characteristics. The analysis should also be improved by solving for the H-force and adding the value to the trim analysis.

The final design of the tail rotor presents characteristics that fulfill the design goals of maximum performance for minimal horsepower required. A problem was discovered when trying to find the power required for thrusts under 200-lbs, the equations no longer work due to the inability to calculate negative collective. Future work needs to be done with negative collective, azimuth sweep for flapping, and hub angle with pitch-flap coupling. Finally, a de-icing system for the tail rotor is planned to fulfill recommendations put forth in the AHS design competition.

IA performed the weight and balance analysis using Prouty's (2002) class II method to achieve the goal of minimizing the CG travel through practical placement of the aircraft's components and people. Although the Class II weight and balance analysis produced a gross weight of approximately 9,500-lbs, IA believes that the E-21 will weigh closer to 10,000-lbs (the max gross weight of the original weight estimate) when a more detailed analysis of other components such as the engine cowlings, fuselage structure, and both the horizontal and vertical stabilizers is conducted.

The trim analysis only took in account the static trim of the aircraft using Prouty's (2002) helicopter trim methods. Some of the difficulties found during the trim analysis include: a

tail rotor and empennage design to counter the main rotor torque and downwash interactions over a range of flight regimes; inability of autorotation analysis; and high main-rotor hub-pitching stiffness limiting the slope landing capability. The trim analysis yielded that the aircraft could be trimmed for the requirement of the 40-kt crosswind from any azimuth while OEI HOGE 12,000-ft Hd. The Aircraft was able to also have a cruise speed of 145-kts. The analysis also showed that IA met the 40-kt crosswind from any azimuth while HOGE at 15,000-ft Hd.

The drag analysis performed followed Prouty's (2002) methods applied to three-dimensions, which included breaking up the fuselage into common shapes with known drag coefficients and extrapolating moment coefficients from Prouty's wind tunnel data. The shapes were gross estimates in conjunction with the three-dimensional application and IA believes that a better drag analysis could be performed with wind tunnel testing.

IA plans to produce 140 helicopters by selling the design of the E-21 to an existing company that produces helicopters due to the high costs for starting a company. A better estimate of the cost of the main rotor and the tail rotor would make cost analysis of the aircraft more accurate. The costs for the extra medical and search equipment carried by the E-21 needs to be incorporated for a more accurate cost analysis.

12.0 REFERENCES

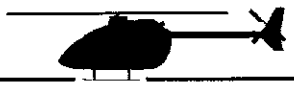

12.1 Cited

Eurocopter, Technical Specifications of the EC 145, Accessed Sep. 15, 2003. <http://www.eurocopter.com>

AIAA, Generic Small Turbo Shaft Engine Data, Accessed Oct. 2003 < http://www.aiaa.org/images/education/11.pdf>

MD Helicopter, Technical Specifications of the MD 900 Explorer Accessed Sep. 15, 2003. < http://www.mdhelicopters.com>

Prouty, Raymond W. (2002). Helicopter Performance, Stability, and Control. Malabar, Florida: Kreiger Publishing Company.

Roskam, J. (1990). Airplane Design Part VIII: Airplane Cost Estimation: Design, Development, Manufacturing, And Operating. Lawrence, Kansas: The University Of Kansas

Stonecipher, J. (Personal Communication, September 2003).

12.2 Non-Cited

Aviation Week and Space Technology (2003). Rotary-Wing Aircraft. 2003 Aerospace Source Manual, 80-89.

Hollmann, E. & Hollmann M, (2001). Modern Helicopter Design. California: Self Published.

Guston, B. (2002). Jane's Aero-Engines, Issue Twelve. Virginia: Jane's Information Group

Leishman, J. Priciples of Helicopter Aerodynamics. Cambridge: Cambridge University Press

Rolls Royce, Accessed Oct. 2003. < http://www.rolls-royce.com>

13.0 APPENDIX A - MISSION SPECS

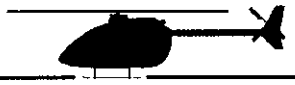

The role of the E-21 helicopter is to perform mountain rescue operations at high altitude. The helicopters that currently support airborne rescue services are developments of existing designs or adaptations of models that are characterized by good high-altitude performance. The E-21 helicopter must be capable of performing a mission consisting of take off from 6000 ft density altitude, 1 hour outbound leg with a crew of 4 at 140 knots, 20 minutes on stations hoist operation with recovery of 2 patients at 12000 ft Density altitude, and 1 hour return leg at 140 knots. The helicopter must be capable of operation in snow.

The helicopters payload consists of medical and search equipment along with passengers and backup power. The medical equipment required is a cardiac monitor, defibrillator, gaseous oxygen, a space E size oxygen cylinder, two packs of advanced life support equipment, and one basket litter. Two engine-driven 200 A, 28 VDC starter generators and 28 V storage battery of capacity sufficient to start engines are also required. A 15 million candlepower searchlight, a 600 lb internal or external hoist, and FLIR/EO stabilized camera system are mandatory search equipment. Two 6-feet 210 lb (185 lb and 25 lb baggage) patients are also a part of the payload.

The crew consists of 2 pilots and 2 paramedics weighing 210 lb each (185 lb and 25 lb baggage).

The E-21 helicopter must be capable of one engine inoperative (OEI) hover out of ground effect (HOGE) at maximum gross weight (MGW) up to 12000 feet Density altitude, International Standard Atmosphere (ISA). The IA must be able to HOGE with all engines operative at MGW up to 15000 feet Density altitude, ISA. The anti-torque system must be capable of maintaining heading in hover with wind from any azimuth up to at least 40 knots at 15000 feet Density altitude. The E-21 has a range of 280 nautical miles. The maximum speed of the IA is 145 knots.

The E-21 must be designed to meet Code of Federal Regulations (CFR) Title 14, Part 29, as applicable according to MTOW or JAR Part 29. The aircraft must be certifiable for single pilot IFR operations.

Table 13.1 – Mission Specification

1.) Engine start and warm up
2.) Taxi
3.) Takeoff from 6000 ft
4.) Climb to 12000 ft
5.) Cruise
6.) Hover
7.) Cruise
8.) Decent
9.) Landing, taxi, shutdown

Figure 13-1 below shows the mission profile for the IA helicopter.

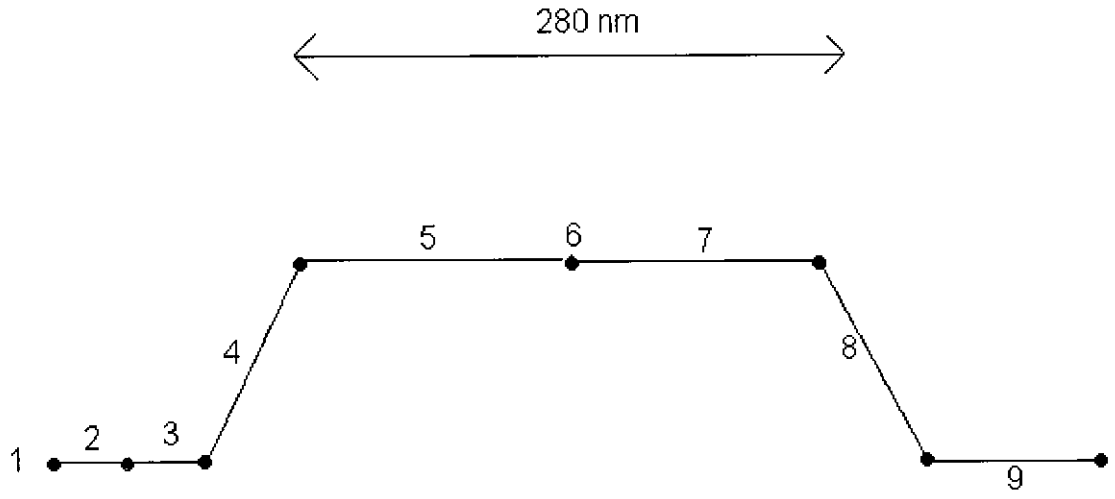

Figure 13-1 – Mission Profile

14.0 APPENDIX B – RAW DATA

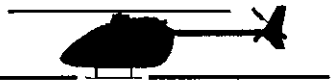

Table 14.1 - CG Empty

CG EMPTY

	Item and Description	Weight	x (ft)	y (ft)	z (ft)	Wx	Wy	Wz
Standard Equipment	Instruments	69.83	3.00	0.00	3.00	209.50	0.00	209.50
	Martin-Baker Passenger Seats pilot # 1	46.00	5.00	0.00	1.50	230.00	0.00	69.00
	Martin-Baker Passenger Seats pilot # 2	46.00	5.00	0.00	1.50	230.00	0.00	69.00
	Martin-Baker Passenger Seats crew # 1	46.00	7.00	0.00	1.50	322.00	0.00	69.00
	Martin-Baker Passenger Seats crew # 2	46.00	7.00	0.00	1.50	322.00	0.00	69.00
	Cockpit Controls	29.00	3.00	0.00	2.00	87.00	0.00	58.00
	Systems Controls	141.00	3.00	0.00	3.00	423.00	0.00	423.00
Avionics	Forward Looking IR (FLIR)	98.00	1.00	0.00	1.75	98.00	0.00	171.50
	Weather Radar (RDR 1400C Telefonics)	44.10	2.00	0.00	1.75	88.20	0.00	77.18
	Radar radome	15.00	0.50	0.00	1.00	7.50	0.00	15.00
	CMA 3000 management system (Canadian Marconi)	16.80	3.00	0.00	3.00	50.40	0.00	50.40
Rescue	Spectrolab SX-5 Starburst 15 mil Candlepower Light	10.00	5.00	0.00	-1.00	50.00	0.00	-10.00
	Rotating Hoist (44301-4 Goodrich)	92.00	11.00	3.00	6.00	1012.00	276.00	552.00
	110VAC Modular Medical System	70.00	14.00	0.00	5.00	980.00	0.00	350.00
	Litter # 1	30.00	12.50	0.00	1.00	375.00	0.00	30.00
	Litter # 2	30.00	12.50	0.00	1.00	375.00	0.00	30.00
Medical	Vital Signs Monitor Adult/Neonatal	8.00	9.00	-2.75	4.00	72.00	-22.00	32.00
	ZOLL PD 1400 Defibrillator	12.00	8.50	-2.75	4.00	102.00	-33.00	48.00
	2200 Liter Capacity Oxygen Tank	25.00	15.00	0.00	5.25	375.00	0.00	131.25
	Liters of Gaseous Oxygen (2882)	9.50	15.00	0.00	5.25	142.50	0.00	49.88
	Spare E Aluminum Oxygen Tank	9.00	6.50	0.00	1.00	58.50	0.00	9.00
	Advanced Life Support Pack	50.00	6.50	-2.75	1.00	325.00	-137.50	50.00
	Misc Storage Bin	15.00	6.50	0.00	0.50	97.50	0.00	7.50
Engines & Tail	Engine # 1	330.00	13.48	0.00	7.69	4448.40	0.00	2537.04
	Engine # 2	330.00	15.40	0.00	8.19	5082.00	0.00	2702.04
	Engine # 3	330.00	13.48	0.00	7.69	4448.40	0.00	2537.04
	Engine Transmission	300.00	10.00	0.00	7.75	3000.00	0.00	2325.00
	Engine Nacelles	258.08	15.41	0.00	7.57	3977.07	0.00	1953.69
	Propulsion Subsystem	278.86	9.00	0.00	8.00	2509.71	0.00	2230.85
	Drive System	640.59	10.00	0.00	6.00	6405.92	0.00	3843.55
	Auxiliary Power Plant	150.00	13.00	0.00	8.63	1950.00	0.00	1293.75
	Hyndraulic System	87.51	8.00	0.00	7.25	700.07	0.00	634.43
	Electrical System	394.00	8.00	0.00	6.00	3152.00	0.00	2364.00
	Air conditioning & Anti-Ice	80.00	14.00	0.00	6.00	1120.00	0.00	480.00
	Hub Weight	300.85	10.00	0.00	12.63	3008.54	0.00	3798.28
	Rotor Weight	414.17	10.00	0.00	12.63	4141.74	0.00	5228.95
	Tail Rotor	59.31	37.50	-1.00	10.50	2224.19	-59.31	622.77
FUEL	Fuel (2000 lbs)	0.00	10.20	0.00	0.50	0.00	0.00	0.00
	Fuel System	78.00	5.00	0.00	0.50	390.00	0.00	39.00
Misc	Manufacturing variation	40.00	0.00	0.00	0.00	0.00	0.00	0.00
	Fuselage Weight	569.64	0.00	0.00	0.00	0.00	0.00	0.00
	Horizontal Stab	36.76	37.00	4.00	10.00	1359.99	147.03	367.56
	Vertical Stab	29.48	37.00	0.00	10.50	1090.74	0.00	309.53
	Landing Gear System	396.00	10.00	0.00	-2.00	3960.00	0.00	-792.00

TOTAL 6061.5

Σ x-moment = 59000.86 ; y-moment= 171.2138 Σ z-moment= 35035.7

x = 9.7337
y = 0.0282
z = 5.7800

Table 14.2 - CG Max Takeoff

CG MAX GROSS TAKEOFF

	Item and Description	Weight	x (ft)	y (ft)	z (ft)	Wx	Wy	Wz
Standard Equipment	Instruments	69.83	3.00	0.00	3.00	209.50	0.00	209.50
	Martin-Baker Passenger Seats pilot # 1	256.00	5.00	0.00	1.50	1280.00	0.00	384.00
	Martin-Baker Passenger Seats pilot # 2	256.00	5.00	0.00	1.50	1280.00	0.00	384.00
	Martin-Baker Passenger Seats crew # 1	256.00	7.00	0.00	1.50	1792.00	0.00	384.00
	Martin-Baker Passenger Seats crew # 2	256.00	7.00	0.00	1.50	1792.00	0.00	384.00
	Cockpit Controls	29.00	3.00	0.00	2.00	87.00	0.00	58.00
	Systems Controls	141.00	3.00	0.00	3.00	423.00	0.00	423.00
Avionics	Forward Looking IR (FLIR)	98.00	1.00	0.00	1.75	98.00	0.00	171.50
	Weather Radar (RDR 1400C Telefonics)	44.10	2.00	0.00	1.75	88.20	0.00	77.18
	Radar radome	15.00	0.50	0.00	1.00	7.50	0.00	15.00
	CMA 3000 management system (Canadian Marconi)	16.80	3.00	0.00	3.00	50.40	0.00	50.40
Rescue	Spectrolab SX-5 Starburst 15 mil Candlepower Light	10.00	5.00	0.00	-1.00	50.00	0.00	-10.00
	Rotating Hoist (44301-4 Goodrich)	92.00	11.00	3.00	6.00	1012.00	276.00	552.00
	110VAC Modular Medical System	70.00	14.00	0.00	5.00	980.00	0.00	350.00
	Litter # 1	240.00	12.50	0.00	1.00	3000.00	0.00	240.00
	Litter # 2	240.00	12.50	0.00	1.00	3000.00	0.00	240.00
Medical	Vital Signs Monitor Adult/Neonatal	8.00	9.00	-2.75	4.00	72.00	-22.00	32.00
	ZOLL PD 1400 Defibrillator	12.00	8.50	-2.75	4.00	102.00	-33.00	48.00
	2200 Liter Capacity Oxygen Tank	25.00	15.00	0.00	5.25	375.00	0.00	131.25
	Liters of Gaseous Oxygen (2882)	9.50	15.00	0.00	5.25	142.50	0.00	49.88
	Spare E Aluminum Oxygen Tank	9.00	6.50	0.00	1.00	58.50	0.00	9.00
	Advanced Life Support Pack	50.00	6.50	-2.75	1.00	325.00	-137.50	50.00
	Misc Storage Bin	15.00	6.50	0.00	0.50	97.50	0.00	7.50
Engines & Tail	Engine # 1	330.00	13.48	0.00	7.69	4448.40	0.00	2537.04
	Engine # 2	330.00	15.40	0.00	8.19	5082.00	0.00	2702.04
	Engine # 3	330.00	13.48	0.00	7.69	4448.40	0.00	2537.04
	Engine Transmission	300.00	10.00	0.00	7.75	3000.00	0.00	2325.00
	Engine Nacelles	258.08	15.41	0.00	7.57	3977.07	0.00	1953.69
	Propulsion Subsystem	278.86	9.00	0.00	8.00	2509.71	0.00	2230.85
	Drive System	640.59	10.00	0.00	6.00	6405.92	0.00	3843.55
	Auxiliary Power Plant	150.00	13.00	0.00	8.63	1950.00	0.00	1293.75
	Hyndraulic System	87.51	8.00	0.00	7.25	700.07	0.00	634.43
	Electrical System	394.00	8.00	0.00	6.00	3152.00	0.00	2364.00
	Air conditioning & Anti-Ice	80.00	14.00	0.00	6.00	1120.00	0.00	480.00
	Hub Weight	300.85	10.00	0.00	12.63	3008.54	0.00	3798.28
	Rotor Weight	414.17	10.00	0.00	12.63	4141.74	0.00	5228.95
	Tail Rotor	59.31	37.50	-1.00	10.50	2224.19	-59.31	622.77
FUEL	Fuel (2000 lbs)	2000.00	10.20	0.00	0.50	20400.00	0.00	1000.00
	Fuel System	78.00	5.00	0.00	0.50	390.00	0.00	39.00
Misc	Manufacturing variation	40.00	0.00	0.00	0.00	0.00	0.00	0.00
	Fuselage Weight	569.64	0.00	0.00	0.00	0.00	0.00	0.00
	Horizontal Stab	36.76	37.00	4.00	10.00	1359.99	147.03	367.56
	Vertical Stab	29.48	37.00	0.00	10.50	1090.74	0.00	309.53
	Landing Gear System	396.00	10.00	0.00	-2.00	3960.00	0.00	-792.00

TOTAL 9321.5

Σ x-moment = 89690.86 : y-moment= 171.2138 Σ z-moment= 37715.7

x = 9.6219
y = 0.0184
z = 4.0461

Table 14.3 - CG In Flight

CG IN-FLIGHT

	Item and Description	Weight	x (ft)	y (ft)	z (ft)	Wx	Wy	Wz
Standard Equipment	Instruments	69.83	3.00	0.00	3.00	209.50	0.00	209.50
	Martin-Baker Passenger Seats pilot # 1	256.00	5.00	0.00	1.50	1280.00	0.00	384.00
	Martin-Baker Passenger Seats pilot # 2	256.00	5.00	0.00	1.50	1280.00	0.00	384.00
	Martin-Baker Passenger Seats crew # 1	256.00	7.00	0.00	1.50	1792.00	0.00	384.00
	Martin-Baker Passenger Seats crew # 2	256.00	7.00	0.00	1.50	1792.00	0.00	384.00
	Cockpit Controls	29.00	3.00	0.00	2.00	87.00	0.00	58.00
	Systems Controls	141.00	3.00	0.00	3.00	423.00	0.00	423.00
Avionics	Forward Looking IR (FLIR)	98.00	1.00	0.00	1.75	98.00	0.00	171.50
	Weather Radar (RDR 1400C Telefonics)	44.10	2.00	0.00	1.75	88.20	0.00	77.18
	Radar radome	15.00	0.50	0.00	1.00	7.50	0.00	15.00
	CMA 3000 management system (Canadian Marconi)	16.80	3.00	0.00	3.00	50.40	0.00	50.40
Rescue	Spectrolab SX-5 Starburst 15 mil Candlepower Light	10.00	5.00	0.00	-1.00	50.00	0.00	-10.00
	Rotating Hoist (44301-4 Goodrich)	92.00	11.00	3.00	6.00	1012.00	276.00	552.00
	110VAC Modular Medical System	70.00	14.00	0.00	5.00	980.00	0.00	350.00
	Litter # 1	240.00	12.50	0.00	1.00	3000.00	0.00	240.00
	Litter # 2	240.00	12.50	0.00	1.00	3000.00	0.00	240.00
Medical	Vital Signs Monitor Adult/Neonatal	8.00	9.00	-2.75	4.00	72.00	-22.00	32.00
	ZOLL PD 1400 Defibrillator	12.00	8.50	-2.75	4.00	102.00	-33.00	48.00
	2200 Liter Capacity Oxygen Tank	25.00	15.00	0.00	5.25	375.00	0.00	131.25
	Liters of Gaseous Oxygen (2882)	9.50	15.00	0.00	5.25	142.50	0.00	49.88
	Spare E Aluminum Oxygen Tank	9.00	6.50	0.00	1.00	58.50	0.00	9.00
	Advanced Life Support Pack	50.00	6.50	-2.75	1.00	325.00	-137.50	50.00
	Misc Storage Bin	15.00	6.50	0.00	0.50	97.50	0.00	7.50
Engines & Tail	Engine # 1	330.00	13.48	0.00	7.69	4448.40	0.00	2537.04
	Engine # 2	330.00	15.40	0.00	8.19	5082.00	0.00	2702.04
	Engine # 3	330.00	13.48	0.00	7.69	4448.40	0.00	2537.04
	Engine Transmission	300.00	10.00	0.00	7.75	3000.00	0.00	2325.00
	Engine Nacelles	258.08	15.41	0.00	7.57	3977.07	0.00	1953.69
	Propulsion Subsystem	278.86	9.00	0.00	8.00	2509.71	0.00	2230.85
	Drive System	640.59	10.00	0.00	6.00	6405.92	0.00	3843.55
	Auxiliary Power Plant	150.00	13.00	0.00	8.63	1950.00	0.00	1293.75
	Hyndraulic System	87.51	8.00	0.00	7.25	700.07	0.00	634.43
	Electrical System	394.00	8.00	0.00	6.00	3152.00	0.00	2364.00
	Air conditioning & Anti-ice	80.00	14.00	0.00	6.00	1120.00	0.00	480.00
	Hub Weight	300.85	10.00	0.00	12.63	3008.54	0.00	3798.28
	Rotor Weight	414.17	10.00	0.00	12.63	4141.74	0.00	5228.95
	Tail Rotor	59.31	37.50	-1.00	10.50	2224.19	-59.31	622.77
FUEL	Fuel (2000 lbs)	2000.00	10.20	0.00	0.50	20400.00	0.00	1000.00
	Fuel System	78.00	5.00	0.00	0.50	390.00	0.00	39.00
Misc	Manufacturing variation	40.00	0.00	0.00	0.00	0.00	0.00	0.00
	Fuselage Weight	569.64	0.00	0.00	0.00	0.00	0.00	0.00
	Horizontal Stab	36.76	37.00	4.00	10.00	1359.99	147.03	367.56
	Vertical Stab	29.48	37.00	0.00	10.50	1090.74	0.00	309.53
	Landing Gear System	396.00	10.00	0.00	-2.00	3960.00	0.00	-792.00

TOTAL **9321.5**

Σ x-moment = 89690.86 ; y-moment= 171.2138 Σ z-moment= 37715.7

x = 9.6219
y = 0.0184
z = 4.0461

Table 14.4 - CG Hover

CG HOVER

	Item and Description	Weight	x (ft)	y (ft)	z (ft)	Wx	Wy	Wz
Standard Equipment	Instruments	69.83	3.00	0.00	3.00	209.50	0.00	209.50
	Martin-Baker Passenger Seats pilot # 1	256.00	5.00	0.00	1.50	1280.00	0.00	384.00
	Martin-Baker Passenger Seats pilot # 2	256.00	5.00	0.00	1.50	1280.00	0.00	384.00
	Martin-Baker Passenger Seats crew # 1	256.00	7.00	0.00	1.50	1792.00	0.00	384.00
	Martin-Baker Passenger Seats crew # 2	46.00	7.00	0.00	1.50	322.00	0.00	69.00
	Man on the Skid	210.00	10.00	4.50	3.50	2100.00	945.00	735.00
	Cockpit Controls	29.00	3.00	0.00	3.00	87.00	0.00	87.00
	Systems Controls	141.00	3.00	0.00	3.00	423.00	0.00	423.00
Avionics	Forward Looking IR (FLIR)	98.00	1.00	0.00	1.75	98.00	0.00	171.50
	Weather Radar (RDR 1400C Telefonics)	44.10	2.00	0.00	1.75	88.20	0.00	77.18
	Radar radome	15.00	0.50	0.00	1.00	7.50	0.00	15.00
	CMA 3000 management system (Canadian Marconi)	16.80	3.00	0.00	3.00	50.40	0.00	50.40
Rescue	Spectrolab SX-5 Starburst 15 mil Candlepower Light	10.00	5.00	0.00	-1.00	50.00	0.00	-10.00
	Rotating Hoist (44301-4 Goodrich)	92.00	11.00	6.00	6.00	1012.00	552.00	552.00
	110VAC Modular Medical System	70.00	14.00	0.00	5.00	980.00	0.00	350.00
	Litter # 1 (victim below)	240.00	11.00	8.00	-50.00	2640.00	1920.00	-12000.00
	Litter # 2 (empty)	30.00	12.50	2.00	1.00	375.00	60.00	30.00
Medical	Vital Signs Monitor Adult/Neonatal	8.00	9.00	-2.75	4.00	72.00	-22.00	32.00
	ZOLL PD 1400 Defibrillator	12.00	8.50	-2.75	4.00	102.00	-33.00	48.00
	2200 Liter Capacity Oxygen Tank	25.00	15.00	0.00	5.25	375.00	0.00	131.25
	Liters of Gaseous Oxygen (2882)	9.50	15.00	0.00	5.25	142.50	0.00	49.88
	Spare E Aluminum Oxygen Tank	9.00	6.50	0.00	1.00	58.50	0.00	9.00
	Advanced Life Support Pack	50.00	6.50	-2.75	1.00	325.00	-137.50	50.00
	Misc Storage Bin	15.00	6.50	0.00	0.50	97.50	0.00	7.50
Engines & Tail	Engine # 1	330.00	13.48	0.00	7.69	4448.40	0.00	2537.04
	Engine # 2	330.00	15.40	0.00	8.19	5082.00	0.00	2702.04
	Engine # 3	330.00	13.48	0.00	7.69	4448.40	0.00	2537.04
	Engine Transmission	300.00	10.00	0.00	7.75	3000.00	0.00	2325.00
	Engine Nacelles	258.08	15.41	0.00	7.57	3977.07	0.00	1953.69
	Propulsion Subsystem	278.86	9.00	0.00	8.00	2509.71	0.00	2230.85
	Drive System	640.59	10.00	0.00	6.00	6405.92	0.00	3843.55
	Auxiliary Power Plant	150.00	13.00	0.00	8.63	1950.00	0.00	1293.75
	Hyndraulic System	87.51	8.00	0.00	7.25	700.07	0.00	634.43
	Electrical System	394.00	8.00	0.00	6.00	3152.00	0.00	2364.00
	Air conditioning & Anti-ice	80.00	14.00	0.00	6.00	1120.00	0.00	480.00
	Hub Weight	300.85	10.00	0.00	12.63	3008.54	0.00	3798.28
	Rotor Weight	414.17	10.00	0.00	12.63	4141.74	0.00	5228.95
	Tail Rotor	59.31	37.50	-1.00	10.50	2224.19	-59.31	622.77
FUEL	Fuel (2000 lbs)	2000.00	10.20	0.00	0.50	20400.00	0.00	1000.00
	Fuel System	78.00	5.00	0.00	0.50	390.00	0.00	39.00
Misc	Manufacturing variation	40.00	0.00	0.00	0.00	0.00	0.00	0.00
	Fuselage Weight	569.64	0.00	0.00	0.00	0.00	0.00	0.00
	Horizontal Stab	36.76	37.00	4.00	10.00	1359.99	147.03	367.56
	Vertical Stab	29.48	37.00	0.00	10.50	1090.74	0.00	309.53
	Landing Gear System	396.00	10.00	0.00	-2.00	3960.00	0.00	-792.00

TOTAL 9111.5

Σ x-moment = 87335.86 Σ y-moment= 3372.214 Σ z-moment= 25714.7

x = 9.5852
y = 0.3701
z = 2.8222

Table 14.5 - Weight Estimates

Weight Estimates

Input Parameters	
b=	5
c=	1.51
R=	23.03
ΩR=	700
J=	2486.50
g=	32.2
A_H=	20
AR_H=	2.875
A_V=	16
AR_V=	1.56
# tail rotor gb=	2
Ω_T=	700
R_T=	3.99
Trans hp rating=	1700
Tail rotor hp rating=	186.22
Ω_M=	30.39
Ω_T=	175.46
GW=	10000
L_F=	20
$Swet_F$=	340.79
EngWt dry=	330
# of eng=	3
$Swet_N$=	152.11
wt. per eng=	330
capacity in gal=	294
# of tanks=	4
rpm_{eng}=	23000
# of gb=	4
# of Wheel Legs	4

Description	Symbol	Weight (lbs)
Main Rotor Blades	W_{bM}=	414.17
Main Rotor Hub & Hinge	W_{hM}=	300.85
Stabilizer (horizontal)	W_H=	36.76
Fin (Vertical stabilizer)	W_V=	29.48
Tail Rotor	W_T=	59.31
Body (fuselage)	W_F=	569.64
Landing Gear	W_{LG}=	395.52
Nacelles	W_N=	258.08
Engine Installation	W_{eng}=	990.00
Propulsion Subsystems	W_{PSS}=	278.86
Fuel System	W_{FS}=	77.50
Drive System	W_{DS}=	640.59
Cockpit Controls	W_{CC}=	28.89
Systems Controls (boosted)	W_{SC}=	141.33
Auxiliary Power Plant	W_{APP}=	150.00
Instruments	W_I=	69.83
Hydraulics	W_{hyd}=	87.51
Electrical	W_{EL}=	393.40
Avionics	W_{av}=	674.70
Furnishings and equipment	W_{FE}=	458.91
Air Conditioning & Anit-ice	$W_{AC\&AI}$=	80.00
Manufacturing Variation	W_{MV}=	40.00

15.0 APPENDIX C – CAD DRAWINGS

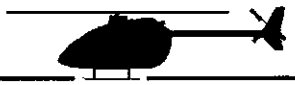

This section contains the following CAD drawings:

Main Cabin Layout
Main Cabin Structural Layout

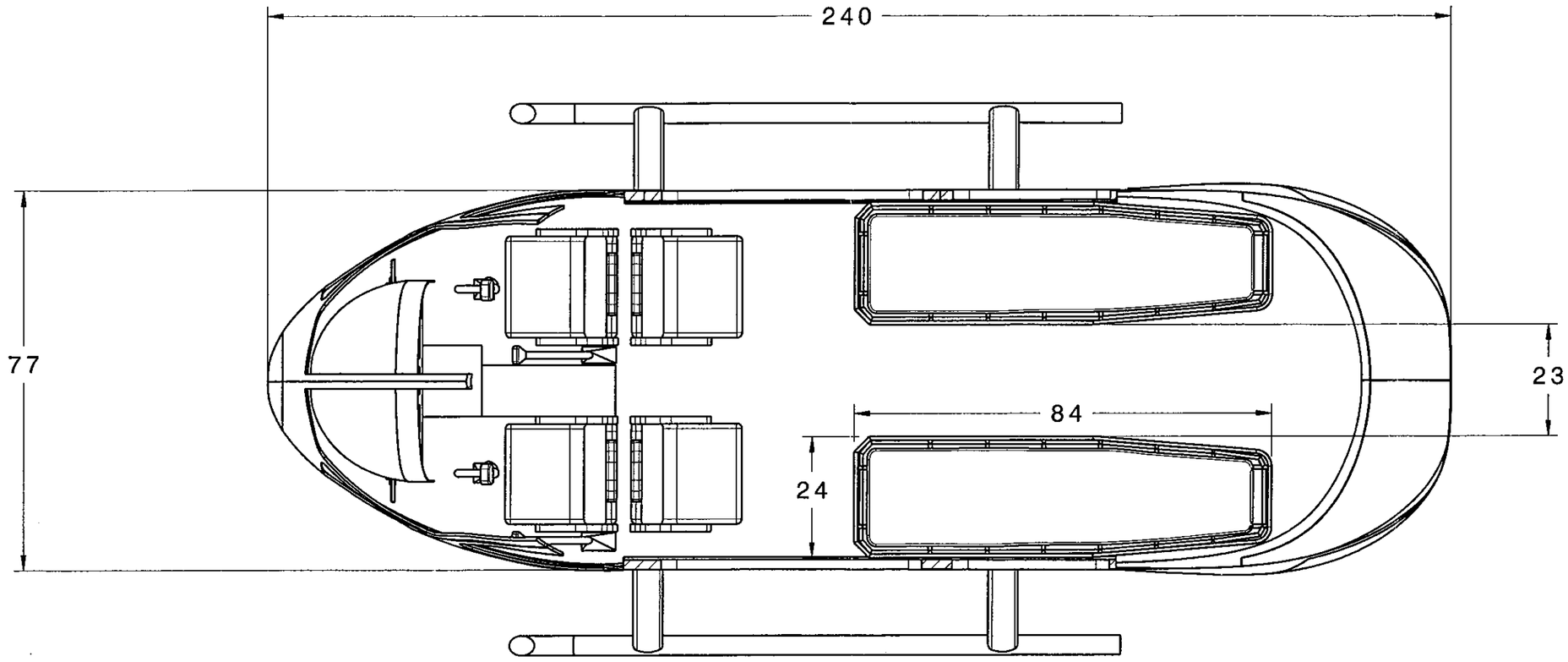

Section A-A

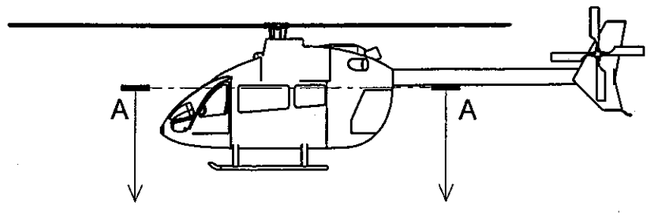

Infinity Aerospace
Embry-Riddle Aeronautical University
3700 Willow Creek Rd.
Prescott, AZ 86301
Aerospace Engineering Dept.

Drawing Discription:

Section View of the Cabin

SIZE	CODE IDENT NO.	8:1 DRAWING NUMBER: 5 OF 7	REVISION
B		DIMENSIONS INCHES	A
		DRAWN BY: BRET DAVENPORT	
SCALE 1 : 25		SPEC:	SHEET: 5 OF 7

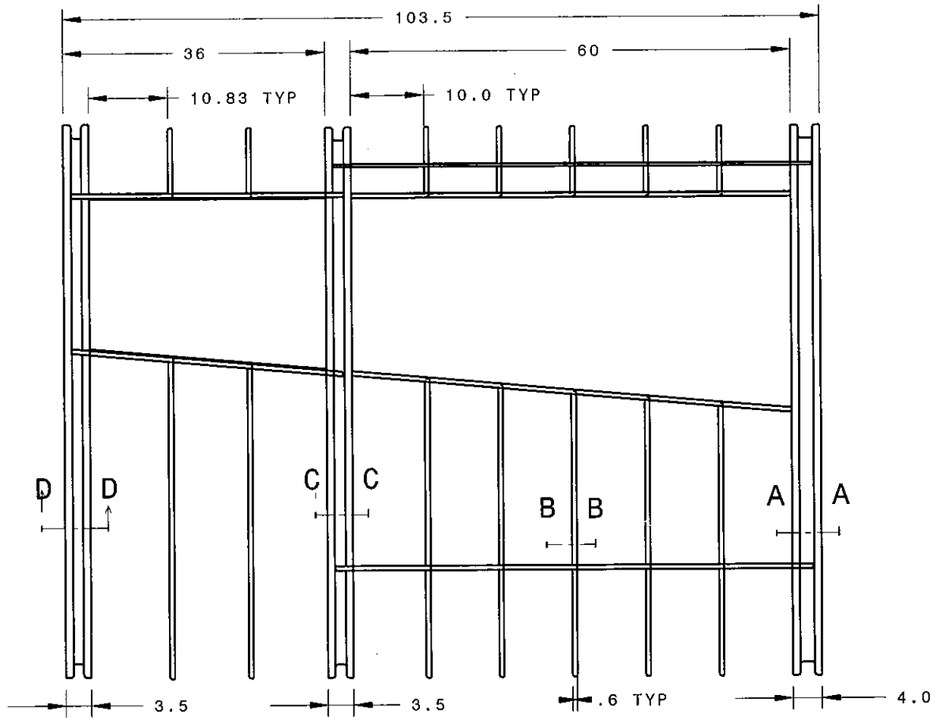

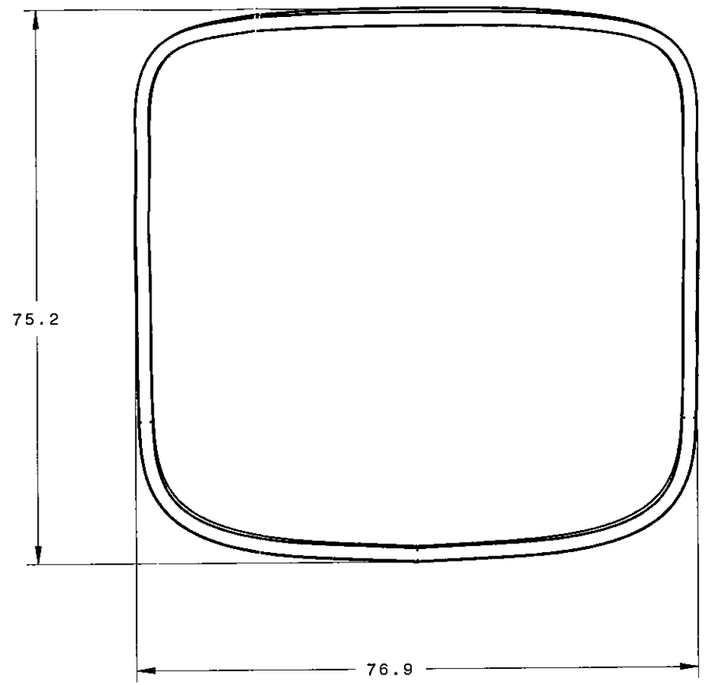

Rear Bulkhead
Section D-D
Scale 1:5

Mid-Bulkhead
Section C-C
Scale 1:5

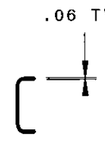

Frame
Section B-B
Scale 1:5

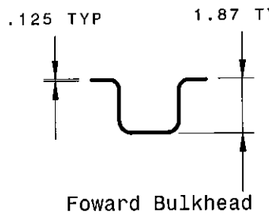

Foward Bulkhead
Section A-A
Scale 1:5

Infinity Aerospace
Embry-Riddle Aeronautical University
3700 Willow Creek Rd.
Prescott, AZ 86301
Aerospace Engineering Dept.

Drawing Discription:

Main Cabin Structural Layout

SIZE	CODE IDENT NO.	8:1 DRAWING NUMBER:	OF	REVISION
B		DIMENSIONS	INCHES	A
		DRAWN BY:	BRET DAVENPORT	
SCALE 1 : 25		SPEC:	SHEET:	OF

16.0 APPENDIX D – PERFORMANCE CHARTS

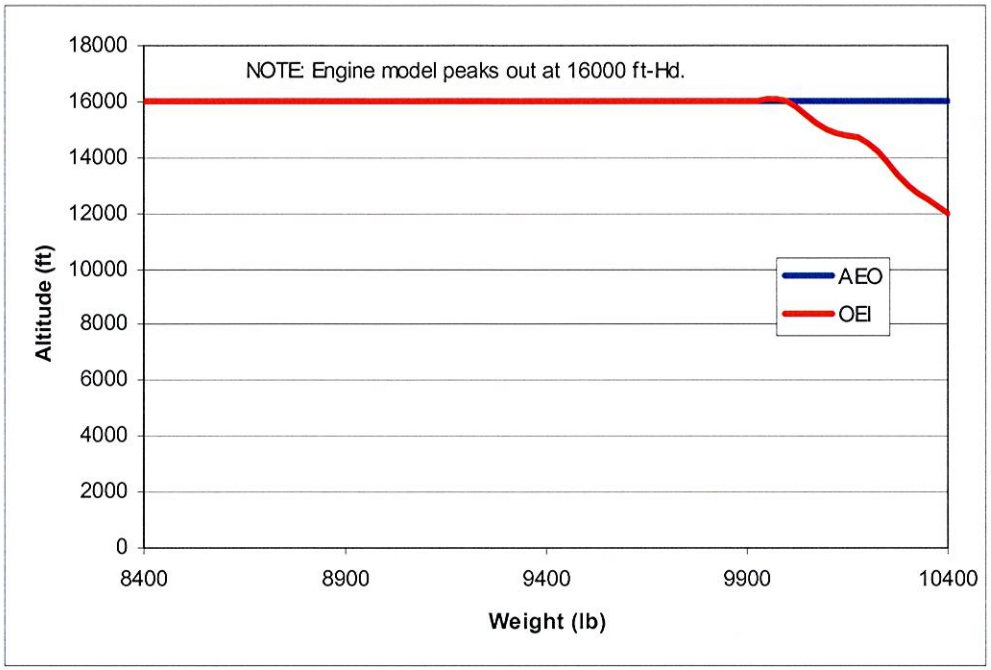

Figure 16-1 - HOGE Altitude vs. Gross Weight

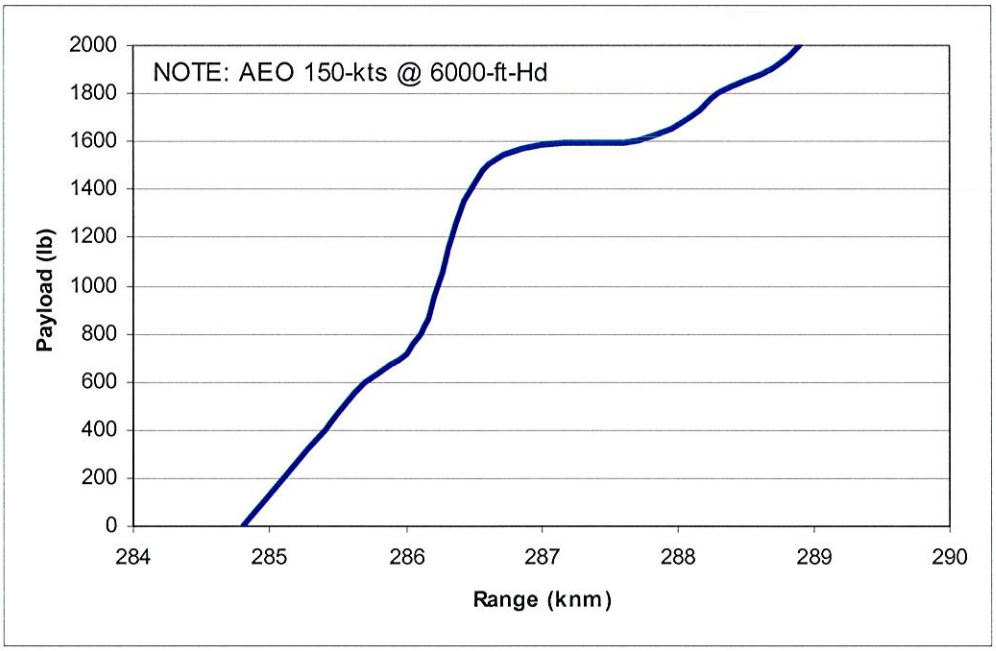

Figure 16-2 - Payload vs. Range at 6000 ft-Hd.

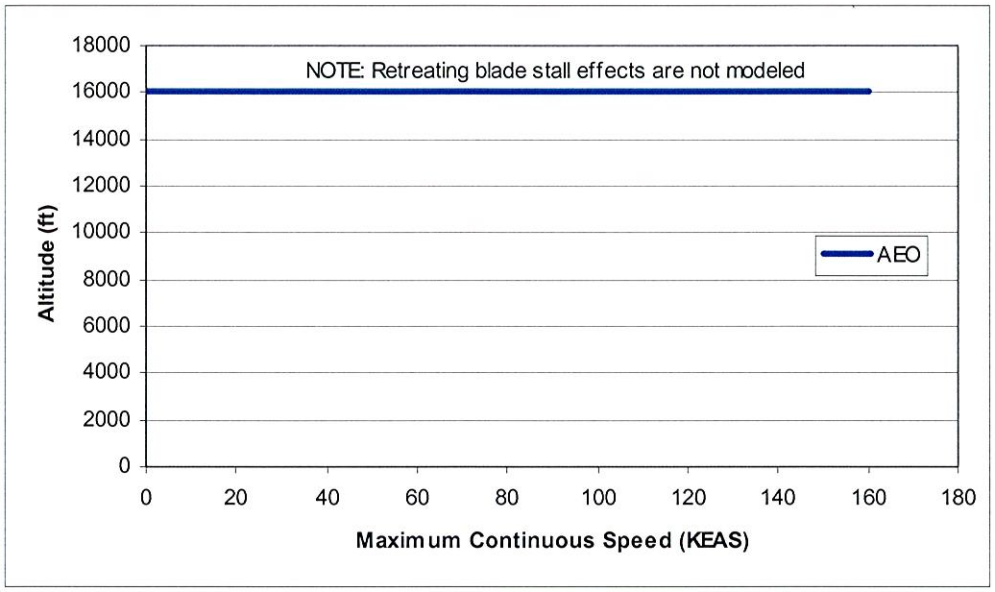

Figure 16-3 - Altitude vs. Maximum Continuous Speed

17.0 APPENDIX E – DYNAMIC MODELING AND SIMULATION

The following is a report covering the dynamic modeling and simulation analysis conducted on the E-21 HAMR.

TABLE OF CONTENTS

1.0 INTRODUCTION

This section discuss IA's attempt to model the E-21 HAMR in order to examine its in-flight characteristics. This was done as an independent study by five members of IA in partial fulfillment of the independent study course designed by Dr. Tom Gally.

The E-21 was modeled by creating several interlinking modules in MATLAB that were later executed with SIMULINK. Each module consisted of an analysis of a major component or critical analysis needed to determine the flight characteristics of the E-21. These modules were:

- Main rotor modules,
- Trim module,
- Fuselage module,
- Tail rotor module,
- Atmospheric density module,
- Weight module,
- Empennage modules.

Once the modules were created, they were later compiled into Flight Gear, an open source flight simulation program. This allowed the members of IA to determine in "real-time" in-flight characteristics.

2.0 THEORY

Understanding a specific helicopter's flight characteristics through the use of dynamic simulation has recently become a valuable asset to design engineers. Through the use of computer program such as MATLAB, a design engineer is able to model his design into a program that will calculate a series of complex algorithms that in turn provides instant feedback on whether or not his design is flawed.

This use of programming is not only valuable, but also cost effective in that full-size test models do not have to be produced in order to test the stability and control characteristics of that particular aircraft. Understanding how the specific helicopter will perform prior to actual tests allows design engineers to modify or correct almost all initial handling problems before they occur. This not only saves, money, but also reduces the loss of human injury that can occur during flight testing.

For the purpose of the E-21 HAMR, several modules were created in MATLAB to help determine its flight characteristics during several flight regimes. These flight regimes include the most sensitive the E-21, hovering out of ground effect (HOGE) at 15,000 feet, density altitude, for the purposes of conducting a rescue operation.

These modules were created for specific components of the E-21 and were then linked together through the use of a control module (the trim module). The modules created analyzed the requirements for the main and tail rotors, the drag of the fuselage, empennage, and flight control inputs necessary to trim the E-21 in flight. The modules allowed several members of IA to determine whether or not the E-21 exhibited desirable flight characteristics in its various flight regimes.

3.0 DISCUSSION MODULES

The following sections will discuss the equations used to create the individual modules used to create the modeling simulation for the E-21 HAMR.

3.1 MAIN ROTOR MODULES

The main rotor modules consisted of two (2) sub-modules that calculated several requirements for E-21's main rotor. One such sub-module was the hover module that utilized the Combined Momentum and Blade Element Theory Method described in Prouty's Helicopter Performance, Stability, and Control (2004). Using the combined momentum and blade element theory, the hover module solved the collective pitch (θ_c) at selected altitudes ranging from sea level to 15,000-ft Hd. The other sub-module was the forward flight module, which utilized a combined method of Blade Element Theory and closed form solutions as is also described in Prouty's Helicopter Performance, Stability, and Control (2004). Both of these modules assumed values for a NACA 0012 airfoil and the methods used in the modules are described in detail in the following sections.

3.2 HOVER MODULE

The purpose of the hover module as the trim module used it, was to provide the collective pitch (θ_c) required to hover at the altitude the helicopter was simulated to be flying at. This value was important to solve for because the equation for the inflow velocity of the air through the main rotor during forward flight is highly dependent on this value. This value was solved by using a combination of Momentum Theory and Blade Element Theory. This section will cover the assumptions and the equations used by these methods in the module.

The first operation completed in the module was the definition of certain properties that were chosen in the preliminary design phase of the helicopter. These properties include the gross weight (G.W.), tip speed (ΩR), disc loading (D.L.), solidity (σ), and the blade number (b). Properties of the blades were also entered in this section including the cutout ratio (x_o), the effective hinge offset (e/R), the lift curve slope of the airfoil (a), the zero lift angle of attack ($C_{l\alpha o}$), and the zero lift drag coefficient (C_{do}). An array of the twist rates on the blades was also entered at this point. These twist rates were developed by manually changing all the twist rates to accomplish the highest lift value for collective pitch. At the end of this section, the values for density (ρ), speed of sound (a_{sound}), and an initial value for collective pitch were read in from the state vector.

The next order of operations in the module was to solve for some of the basic geometries and values of the rotor system that could be derived from equations using the previously stated properties. The radius (R) of the rotor disc was solved using Momentum Theory and the values of gross weight and disc loading in the formula displayed in Equation 3.2.1:

$$R = \sqrt{\frac{G.W.}{\frac{D.L.}{\pi}}} \qquad \text{Equation 3.2.1}$$

The area of the disc was then solved using the basic formula that is displayed below in Equation 3.2.2:

$$A = \pi R^2 \qquad \text{Equation 3.2.2}$$

Both of these values were then used alongside the solidity and blade number to find the chord length (c) of the blades using the formula in Equation 3.2.3:

$$c = \frac{A \times \sigma}{R \times b} \qquad \text{Equation 3.2.3}$$

The chord length of the main rotor was chosen to be constant in the preliminary design phase in an attempt to alleviate some of the complication in the design of the main rotor. The angular velocity (Ω) of the rotor was solved using a basic equation from dynamics principles that is shown in Equation 3.2.4:

$$\Omega = \frac{\Omega R}{R} \qquad \text{Equation 3.2.4}$$

The values found from the previous equations and properties were then used in the portion of the module that utilized Blade Element Theory. Blade Element Theory works off of the assumption that the rotor blade can be separated into many portions, or blade stations as they are officially termed. The entire rotor blade is divided in this manner because the rotor blade experiences increasing linear velocity along its length. The change in velocity coupled with the twist in the blade acts to change the lift and drag values along the length of the rotor blade. The principles of aerodynamic lift and drag are applied to all of these various blade stations and combined to determine values for the entire blade, such as thrust, torque and the horsepower required to rotate the blade. Put simply, Blade Element Theory is a rudimentary form of integrating the values of lift and drag along the length of a rotor blade.

The hover module uses a for-loop to solve for the required properties at each blade station. Prouty suggests that the blade be separated into fifteen (15) blade stations to calculate the lift distributions with any reasonable accuracy. Therefore, the for-loop was made to loop fifteen (15) times to account for each blade station. Two (2) for-loops were constructed in the module due to one of the results calculated in the first loop being the tip loss. This value was applied to the calculations found in the second loop, so that a fairly accurate model of losses could be used for each blade.

Each loop had the same basic setup, starting with the calculation of the linear percentage of the rotor blade (r/R) that each blade station was acting at. This was done by dividing

the loop number (r), which represented a linear distance from the hub, by 15 such that when the last station was reached a value of one hundred percent would be attained. The twist at each blade station was then calculated using the formula shown on the following page in Equation 3.2.5:

$$\text{Twist} = \frac{\text{r}}{\text{R}} \times \text{Twist Rate} + \text{Previous Twist} \qquad \text{Equation 3.2.5}$$

The variable Previous Twist was initialized outside of the loop to a value of zero because it was assumed that there was no initial twist of the blades at the rotor hub. From this value, the pitch (θ) of the blade station could then be found using the formula in the Equation 3.2.6:

$$\theta = \theta_0 + twist - \text{C}_{\ell_{\alpha 0}} \qquad \text{Equation 3.2.6}$$

The mach number of the blade station was then calculated so that the lift curve slope could later be corrected for that mach number. This was solved using the formula shown in Equation 3.2.7:

$$\text{M} = \frac{\frac{\text{r}}{\text{R}} \times \Omega R}{\text{speed of sound}} \qquad \text{Equation 3.2.7}$$

This value was then used to calculate the corrected lift curve slope ($C_{l\alpha o}$) using the formula displayed in Equation 3.1.8:

$$\text{C}_{\ell_a} = \frac{a}{\sqrt{1 - M^2}} \qquad \text{Equation 3.2.8}$$

One of the most important values found in the loops is the inflow velocity (v_{1hov}) at each blade station. As was stated before, the hover collective pitch is used in the forward flight module to find the inflow velocity during forward flight. This was performed by calculating the inflow velocity during hover, and then altering the value with the forward flight velocity. The collective pitch directly affected the equation used to solve for inflow velocity by changing the pitch of the blades. This value can be seen in the formula displayed in Equation 3.2.9:

$$v_{1hov} = \frac{\frac{-\Omega}{2} acb + \sqrt{\left(\frac{\Omega}{2} acb\right)^2 + 8\pi b \Omega^2 ra\theta_c}}{8\pi} \qquad \text{Equation 3.2.9}$$

This value was then used to solve for the inflow velocity angle (ϕ) using the formula in Equation 3.2.10:

$$\phi = \frac{v_1}{\Omega r}$$ Equation3.2.10

This value was then used to find the angle of attack (α) of the blade station with the use of the formula shown in Equation 3.2.11:

$$\alpha = \theta - \frac{v_1}{\Omega r}$$ Equation 3.2.11

The value found for angle of attack was then used to find both the lift and drag coefficient for the blade station using Equation 3.2.12 and Equation 3.2.13:

$$C_\ell = \alpha \times C_{\ell\alpha}$$ Equation 3.2.12

$$C_d = C_{d_0} + AC_\ell^{\,2}$$ Equation 3.2.13

These two variables were used in the first loop to solve for the thrust coefficient of the rotor blade without tip loss, and the profile torque coefficient, which doesn't take into account any losses. The equation for the running thrust coefficient is shown in Equation 3.2.14:

$$\frac{dC_T}{d\frac{r}{R}} = \frac{\left(\frac{r}{R}\right)^2 \sigma C_\ell}{2}$$ Equation 3.2.14

This value had to be integrated over the blade using the formula in Equation 3.2.15:

$$C_{T_{No\ Tiploss}} = \int_{x_0}^{1} \frac{dC_T}{d\frac{r}{R}} d\frac{r}{R}$$ Equation 3.2.15

Therefore, the formula in Equation 3.2.14 was multiplied by the length of the blade section, which ended up being $1/15^{th}$ of the blade radius. An if-statement was entered into the loop such that any value of r/R that was less than the cutout ratio would be given a value of zero. These values were added up at the end of the loop to find the total thrust coefficient without tip loss. The profile torque coefficient (C_{Q0}) was solved for in the same manner except no root losses were taken into account. The formulas used to solve for the profile torque coefficient are shown in Equation 3.2.16 and Equation 3.2.17 on the following page.

$$\frac{dC_{Q_0}}{d\frac{r}{R}} = \frac{\left(\frac{r}{R}\right)^3 \sigma C_d}{2}$$ Equation 3.2.16

$$C_{Q_0} = \int_0^1 \frac{dC_{Q_0}}{d\frac{r}{R}} d\frac{r}{R}$$ Equation 3.2.17

At the end of the first loop the tip loss factor (B) was solved for using the formula shown in Equation 3.2.18:

$$B = 1 - \frac{\sqrt{2 \times C_{T_{No\ Tiploss}}}}{b}$$ Equation 3.2.18

This value was used in the second loop to solve for thrust coefficient with tip losses using the same formula as the first loop to solve for the thrust coefficient, except any value less than B was assigned a value of zero. The resultant value was then used to find the total thrust coefficient using the formula shown in Equation 3.2.19:

$$C_T = C_{T_{No\ Tiploss}} - \int_B^1 \frac{dC_T}{d\frac{r}{R}} d\frac{r}{R}$$ Equation 3.2.19

The induced torque coefficient (C_{Qi}) was solved in the same manner as the other coefficients with both root and tip losses taken out with if-statements. The formulas used, which are similar to the others are shown in Equation 3.2.20 and Equation 3.2.21:

$$\frac{dC_{Q_i}}{d\frac{r}{R}} = \frac{\left(\frac{r}{R}\right)^3 \sigma C_\ell \frac{v_1}{\Omega R}}{2}$$ Equation 3.2.20

$$C_{Q_i} = \int_{r_0}^{B} \frac{dC_{Q_i}}{d\frac{r}{R}} d\frac{r}{R}$$ Equation 3.2.21

At this point the module calculates the change in the induced torque coefficient due to the rotation of the wake. The induced power ratio for this rotor system was found using a chart in Prouty's book to be 0.022. This was used to find the change in the induced torque coefficient with the formula shown in Equation 3.2.22:

$$\Delta C_{Q_i} = \text{induced power ratio} \times C_{Q_i} \qquad \text{Equation 3.2.22}$$

The correction factor for the torque coefficient was found using another chart in Prouty's book to have a value of 1.07. This was used to find the total torque coefficient using the formula found on the following page in Equation 2.2.23:

$$C_Q = \left(C_{Q_o} + C_{Q_i} + \Delta C_{Q_i}\right) \times \text{correction factor} \qquad \text{Equation 3.2.23}$$

At this point the thrust (T), torque (Q) and horsepower (h.p.) of the main rotor were calculated using the formulas in Equation 3.2.24, Equation 3.2.25, and Equation 3.2.26:

$$T = \rho A(\Omega R)^2 C_T \qquad \text{Equation 3.2.24}$$

$$Q = C_Q \rho A(\Omega R)^2 R \qquad \text{Equation 3.2.25}$$

$$h.p. = \frac{\rho A(\Omega R)^3 C_Q}{550} \qquad \text{Equation 3.2.26}$$

The collective pitch required to hover was solved for with the use of a control module that was built for the hover module. This module used a Newton Iteration method to drive the thrust of the main rotor equal to the weight of the helicopter. It did this by using the collective pitch as the variable it changed. This value was then passed to the forward flight module so it could perform its job.

3.3 FORWARD FLIGHT MODULE

The purpose of the forward flight module as the trim module used it, was to provide the resultant thrust vector from the main rotor due to the cyclic and collective inputs. This value was important to solve for because it is used to find the flight velocity and direction the helicopter is flying in. The module is also used to calculate the torque produced by the main rotor, so the tail rotor module would be able to produce the proper amount of counteracting thrust. These values are solved using a combination of Blade Element Theory and closed form flapping equations. This section will cover the assumptions and the equations used by these methods in the module.

The first operation completed in the module was the definition of certain properties that were chosen in the preliminary design phase of the helicopter, just as was done in the hover module. The same values were defined, with the addition of a linear blade twist assumption (θ_1), the mast height above the CG (h_m), the lateral mast offset (y_m), the longitudinal mast offset (l_m), the mast incidence (i_m), the lock number (γ), and the acceleration due to gravity (g). The value for the hub pitching stiffness (dR/db_{1s} and dM/da_{1s}) as was solved in the preliminary design phase was also entered in this section. Also in this section, the values for density (ρ), speed of sound (a_{sound}), the values for

hover and forward flight collective pitch, the three (3) velocity values (V_x, V_y, and V_z), and the pitch body angle (Θ) were read in from the state vector. From the three (3) velocity values, flight velocity was calculated using the formula shown on the following page in Equation 3.2.27:

$$V = \sqrt{V_x^2 + V_y^2 + V_z^2} \qquad \text{Equation 3.3.27}$$

The sideslip angle (β) was then calculated using the components of velocity and the resultant velocity vector as shown in the formula in Equation 3.3.28:

$$\beta = \sin^{-1}\left(\frac{-V_y}{V}\right) \qquad \text{Equation 3.3.28}$$

The helicopter angle of attack (α_c) was calculated using the components of velocity and the resultant velocity vector as shown in the formula in Equation 3.3.29:

$$\alpha_c = \sin^{-1}\left(\frac{-V_z}{V}\right) \qquad \text{Equation 3.3.29}$$

The flight path angle of the helicopter (γ_c) was calculated using the difference between Θ and α_c as is shown in Equation 3.3.30:

$$\gamma_c = \Theta - \alpha_c \qquad \text{Equation 3.3.30}$$

The advance ratio (μ), which is a non-dimensionalized form of the forward flight velocity through the rotor system, was calculated assuming small angles with formula displayed in Equation 3.3.31:

$$\mu = \frac{V}{\Omega R} \qquad \text{Equation 3.3.31}$$

When these values had been calculated, the module was ready to start the integration loops for calculating the thrust and torque of the rotor blades. In order for flapping angles to be calculated inside the module with the use of closed form equations, an initial thrust coefficient had to be estimated, and with a while-loop it drives the thrust coefficient to an equilibrium value between the initial value and calculated value. This thrust coefficient was assumed to be the thrust equal to the weight of the helicopter with the use of the formula in Equation 3.3.32:

$$C_T = \frac{G.W.}{\rho \pi R^4 \Omega^2} \qquad \text{Equation 3.3.32}$$

Outside the while-loop, the inflow ratio (λ') was assumed to be zero, such that calculations could be performed. The calculation of the flapping angles was then

performed within the while-loop before the integration loops began. The first value calculated in this section was the inflow velocity through the main rotor, using the formula shown on the following page in Equation 3.3.33:

$$v_1 = \frac{-V^2}{2} + \sqrt{\frac{V^4}{4} + \left(\frac{C_T[\Omega R]^2}{2}\right)^2} \qquad \text{Equation 3.3.33}$$

The coning angle (a_o) was calculated using the formula shown in Equation 3.3.34:

$$a_o = \frac{2\gamma C_T}{3\sigma a} - \frac{3g}{2R\Omega^2} \qquad \text{Equation 3.3.34}$$

The lateral and longitudinal cyclic (A_1 and B_1) values were read in at this point from the state vector, and were used in the equations for the lateral and longitudinal flapping angles (b_{1s} and a_{1s}) as shown in Equation 3.3.35 and Equation 3.3.36 respectively:

$$b_{1s} = A_1 + \frac{\left(a_o\left[\frac{4}{3}\mu + \frac{16\mu^4}{45\pi}\right] + \frac{v_1}{\Omega R}\left[1 + \frac{\mu^4}{24}\right]\right)}{\left(1 + \frac{\mu^2}{2} - \frac{\mu^4}{24}\right)} \qquad \text{Equation 3.3.35}$$

$$a_{1s} = -B_1 + \frac{\mu\left(\theta_o\left[\frac{8}{3}\mu + 32\frac{16\mu^3}{45\pi}\right] + \left[2 + \frac{\mu^4}{12}\right]\theta_o + \lambda\left[2 - \frac{\mu^2}{2}\right]\right)}{\left(1 + \frac{3\mu^2}{2} - \frac{5\mu^4}{24}\right)} \qquad \text{Equation 3.3.36}$$

Once the flapping angles were calculated, the tip path plane angle of attack (α_{TPP}) was calculated using the formula in Equation 3.3.37:

$$a_{TPP} = \Theta + i_m + a_{1s} - \gamma_c \qquad \text{Equation 3.3.37}$$

After this was calculated, λ' was then calculated using the formula in Equation 3.3.38:

$$\lambda' = \mu\alpha_{TPP} - \frac{v_1}{\Omega R} \qquad \text{Equation 3.3.38}$$

The for-loops for the integration of the rotor blades were then begun. The method used for integration followed a similar pattern to that in the hover module. As in the hover module, the lift and drag was found along the entire length of the blade using fifteen (15) blade elements. The difference is that these properties were solved at sixteen (16)

azimuth angles around the rotor head. This was done so that the lift differentiation in the disc could be accounted for. To accomplish these tasks, two (2) for-loops were built.

The inner loop was built to solve for the thrust coefficient, torque coefficient and the H-force coefficient at each blade azimuth position, and the outer loop was built to cycle through the azimuth positions. The first loop began by using Equation 3.2.5 through Equation 3.2.9 like the two hover for-loops. At this point the velocity at the rotor blades was non-dimensionalized into vector form as the tangential velocity (U_T), the perpendicular velocity (U_p), the resultant velocity from the tangential and perpendicular velocities (U_B), and the radial velocity (U_R). The formulas for these properties are displayed in Equation 3.3.39 through Equation 3.3.42:

$$\overline{U}_T = \frac{r}{R} + \mu\sin(\psi+\beta) \qquad \text{Equation 3.3.39}$$

$$\overline{U}_P = \mu(\alpha_{TPP} - a_{1s}) - \frac{\sqrt{\frac{-v^2}{2} + \sqrt{\frac{v^4}{4} + v_{1hov}{}^4}}}{\Omega r} \times \frac{r}{R}\left(1 + \min\left(1, \frac{v_{(Kts)}}{34}\right) \times \frac{r}{R}\cos(\psi+\beta)\right)$$
$$-\frac{r}{R}(a_{1s}\sin\psi - b_{1s}\cos\psi) - \mu(a_0 - a_{1s}\cos\psi - b_{1s})\cos(\psi+\beta)$$
$$\text{Equation 3.3.40}$$

$$\overline{U}_b = \sqrt{\overline{U}_T{}^2 + \overline{U}_P{}^2} \qquad \text{Equation 3.3.41}$$

$$\overline{U}_R = \mu\cos(\psi+\beta) \qquad \text{Equation 3.3.42}$$

As can be seen in Equation 3.3.40 a minimum function is used below 34-kts to keep the equation for perpendicular velocity from "blowing up" at velocities below that value. The equation was found to cause the torque to become unreasonably high below 34-kts during the preliminary design phase of the helicopter, so this linear limit was put on the equation. This is a very large assumption, and a better curve should be put in place to form a more accurate value at low velocities. It can also be seen that the sideslip angle is taken into account by adding it to the azimuth angle (ψ) where blade position was used in the function. This was not initially found in Prouty's equations, but was added in to allow various flight paths to be investigated.

The angle of attack of the blade element was then calculated using the formula shown in Equation 3.3.43:

$$\alpha = \Theta_0 + \text{twist} - C\ell_{\alpha 0} - A_1\cos\psi - B_1\sin\psi + \tan^{-1}\left(\frac{\overline{U}_P}{\overline{U}_T}\right) \qquad \text{Equation 3.3.43}$$

Another large assumption was made at this point to keep the angle of attack from becoming unreasonable, which was done by performing a recommendation given in Prouty's book. An if-statement was made that adds 2π to the resultant solution if the tangential velocity is negative. The lift coefficient of the blades was calculated using the formula shown in Equation 3.3.44:

$$C\ell = \alpha \left(\frac{a}{\sqrt{1 - \left(\frac{\bar{U}_b \Omega R}{a} \right)^2}} \right) \qquad \text{Equation 3.3.44}$$

The lift coefficient was assumed to never go above a value of 2, so an if-statement was made to assign a value of 2 to any value that resulted as greater than 2. A better value for the lift coefficient could be found if a model of the airfoil data could be built into the module.

The drag coefficient was calculated using the same formula as was previously shown in Equation 3.3.13. This value and the lift coefficient value were used to calculate the normal force coefficient with the use of the formula in Equation 3.3.45:

$$C_N = C_\ell \left(\frac{\bar{U}_T}{\bar{U}_b} \right) + C_d \left(\frac{\bar{U}_P}{\bar{U}_b} \right) \qquad \text{Equation 3.3.45}$$

The skin friction drag (c_f) was assumed to have a value of 0.006, therefore the pressure drag (c_{dp}) was simply calculated using the formula in Equation 3.3.46:

$$c_{d_p} = c_d - 0.006 \qquad \text{Equation 3.3.46}$$

From these values, the total chordwise coefficient (c_{co}) and the induced chordwise coefficient (c_{cind}) were solved using the formulas in Equation 3.3.47 and Equation 3.3.48 respectively:

$$C_{C_0} = C_{dP} \frac{\bar{U}_P}{\bar{U}_B} + C_f \left(\frac{\bar{U}_T \sqrt{\bar{U}_T^{\,2} + \bar{U}_R^{\,2}}}{\bar{U}_B^{\,2}} \right) \qquad \text{Equation 3.3.47}$$

$$c_{c_{ind}} = -C_\ell \frac{\bar{U}_P}{\bar{U}_B} \qquad \text{Equation 3.3.48}$$

These values were then used to solve for the coefficients of the different components of torque and the H-force coefficient. The method used for the following equations was the same method as was described for solving for the thrust coefficient in the hover module.

$$C_T/\sigma = \int_{x_0}^{B} \frac{d\,C_T/\sigma}{d\,r/R}\, d\,\frac{r}{R}$$ Equation 3.3.56

The values solved in each equation are added to the corresponding values as the loop continues, and at the end of the loop, the values are added in the outer loop. When all sixteen (16) azimuth angles have been run, the average of each value is found and assumed to be the correct value for the total disc. It is at this point that the resultant thrust coefficient is compared with the initial assumption. If the values are more than 0.0000001 different, the while-loop is run through again. The thrust, torque and H-force values are then calculated using the formulas described in Equation 3.2.24 and Equation 3.2.25, with the H-force being solved with the same equation as the thrust, using the H-force coefficient instead of the thrust coefficient.

The last operation performed in the module is to solve for the resultant forces and moments produced by the main rotor. The equations for the X, Y, and Z components of the resultant forces are shown in Equation 3.3.57 through Equation 3.3.59:

$$X = -H\cos(a_{1s} + i_m) - T\sin(a_{1s} + i_m)$$ Equation 3.3.57

$$Y = T\sin(b_{1s}) - H\sin(\beta)$$ Equation 3.3.58

$$Z = -T\cos(a_{1s} + i_m)$$ Equation 3.3.59

The equations for the L, M, and N components of the resultant moments are shown in Equation 3.3.60 through Equation 3.3.62:

$$L = \frac{dR}{db_{1s}} b_{1s} + Q\sin(a_{1s} + i_m) + Yh_m + Zy_m$$ Equation 3.3.60

$$M = \frac{dR}{da_{1s}} a_{1s} + Q\sin(b_{1s}) + Xh_m + Zl_m$$ Equation 3.3.61

$$N = Q\sin(a_{1s} + i_m)\cos(b_{1s}) - Yl_m$$ Equation 3.3.62

These values were then passed to the trim module, that used to find the new flight velocity of the helicopter. It is recommended that a better representation of airfoil data be used for the forward flight module. This would produce a more accurate representation of aerodynamic forces acting on the rotor blades.

3.4 TRIM MODULE

A trim module was created with the assistance of Dr. Gally to meet the specific demands of IA. The axis in which the trim module used was oriented such that the positive x-axis was out of the nose. This convention followed Prouty's right-hand coordinate system. This module controlled an array of thirteen (13) variables by calculating the forces and moments received from the other flight modules. Depending on the forces and moments calculated, the trim module adjusted each of the thirteen variables accordingly until a desired state of forces and moments was reached.

The main force moment module controlled an array of six variables, which represented the forces along the X, Y, and Z-axes, and the moments about the X, Y, and Z-axes. The trim module assumed that only one variable affected each of these forces and moments and adjusted that one variable until the desired force or moment reached zero. The next variable was then manipulated in a similar fashion. The variable that controlled force in the X direction was body pitch angle. The variable that controlled force in Y direction was body roll angle. The variable that controlled force in Z direction was main rotor collective angle. The variable that controlled moment about the X-axis was lateral cyclic. The variable that controlled moment about the Y-axis was longitudinal cyclic. The variable that controlled moment about the Z-axis was tail rotor collective. For example when the trim module wanted to solve for the force in the X direction to be zero it did that by changing the body pitch angle. This returned a six-by-six diagonal matrix which was solved by using a Newton Iteration for each variable, until the change in the forces and moments was zero. This matrix multiplication is shown in Equation 3.4.1

$$\begin{bmatrix} \partial X/\partial\theta & 0 & 0 & 0 & 0 & 0 \\ 0 & \partial Y/\partial\phi & 0 & 0 & 0 & 0 \\ 0 & 0 & \partial Z/\partial\theta_0 & 0 & 0 & 0 \\ 0 & 0 & 0 & \partial L/\partial A_1 & 0 & 0 \\ 0 & 0 & 0 & 0 & \partial M/\partial B_1 & 0 \\ 0 & 0 & 0 & 0 & 0 & \partial N/\partial\theta_{0t} \end{bmatrix} \begin{Bmatrix} \Delta\theta \\ \Delta\phi \\ \Delta\theta_0 \\ \Delta A_1 \\ \Delta B_1 \\ \Delta\theta_{0t} \end{Bmatrix} = \begin{Bmatrix} -X \\ -Y \\ -Z \\ -L \\ -M \\ -N \end{Bmatrix}$$

Equation 3.4.1

3.5 FUSELAGE MODULE

The fuselage module calculated fuselage drag experienced by the E-21 in direction. This module used the method of sections applied to the top, side, and front of the helicopter. Each section was assigned a drag coefficient according to their respective shape. The corresponding areas and the dynamics pressure were then multiplied by the respective drag coefficient. Using process, IA was able to determine an estimated drag force for the overall helicopter.

IA assumed that drag on the top was equal to the drag on the bottom portion of the helicopter as well as drag on the right being equal to the drag on the left. Also, the drag backwards was equal to the drag experienced in the front of the helicopter. Using these assumptions, trigonometry was then used to calculate the drag force from any given direction and altitude.

3.6 TAIL ROTOR MODULE

The tail rotor module was created in a similar fashion as the main rotor hover module. The parameters of the tail rotor were inputted into the modified hover module that then calculated the pitch angle of the tail rotor blades.

The same calculations were used in the tail rotor module as used in the main rotor modules.

3.7 ATMOSPHERIC DENSITY MODULE

An atmospheric density module was created in order to calculate the various atmospheric densities that the E-21 would fly through. Since atmosphere varies according to altitude, the power requirements for the E-21 also vary. The atmospheric density calculator allowed members of IA to determine the minimum power requirements needed for the E-21 at the various flight regimes it would fly at. One critical altitude was the 15,000-ft which required the most power output from the E-21. This model was constructed from the standard atmospheric lapse rates found the 1976 Standard Atmospheric Density Calculator (US Standard Atmosphere 1976). The altitude was imported into the calculator and then converted from standard units to metric units. From this, the temperature, density, and pressure were calculated. Standard sea level values were used to calculate these values at different altitudes. The initial values at sea level are the following:

- Temperature, $T_0 = 288.15$-K
- Density, $\rho_0 = 1.225$-kg/m^3
- Pressure, $P_0 = 101325$-N/m^2

Since the E-21 only travels up to 15,000-ft, the E-21 only travels through the troposphere. The troposphere goes from sea level to 11,000-m. The temperature was found by inputting the altitude (h) into Equation 3.7.1:

$$T = T_0\left(1 - \frac{h}{44329}\right) \qquad \text{Equation 3.7.1}$$

The density was found using Equation 3.7.2 and the pressure was found using Equation 3.7.3:

$$\rho = \rho_0\left(1 - \frac{h}{44329}\right)^{4.2558} \qquad \text{Equation 3.7.2}$$

$$P = P_0\left(1 - \frac{h}{44329}\right)^{5.255876} \qquad \text{Equation 3.7.3}$$

The values found from these equations were then converted from metric back to standard units. These values were then given back to the function that called this module.

3.8 WEIGHT MODULE

The weight module was created using Prouty's equations on weights due to body angles (Prouty 2004). These body angles were pitch (Θ), roll (Φ) and yaw (Ψ). Weight (W) components were found for each aerodynamic force and moment. The moments are zero because these weight components act through the center of gravity (CG). The aerodynamic force components from the weight was found using the following equations:

$$X = -W*\sin(\Theta) \qquad \text{Equation 3.8.1}$$

$$Y = W*\sin(\Phi)*\cos(\Theta) \qquad \text{Equation 2.8.2}$$

$$Z = W*\cos(\Theta)*\cos(\Phi) \qquad \text{Equation 2.8.3}$$

This module was also used by trim module to calculate the force and moments experienced by the E-21.

Two assumptions were used during the creation of this module. The first assumption was that the weight of the helicopter remained constant. That is, during the flight of the E-21, IA did not take into account the decrease in weight as fuel was expended. The second assumption was the center of gravity did not move. This was directly related to the fact that the module does not account for fuel burn. Although the CG does not move much longitudinally or laterally, the vertical position moves three feet upwards as the helicopter consumed fuel.

3.9 EMPENNAGE MODULES

The empennage of the E-21 was broken down into two (2) sub-modules, the vertical tail module (VerticalEmpennage) and the horizontal tail module (HorizontalEmpennage). Both the vertical and the horizontal tails are composed of NACA 0012 airfoils and made to calculate results for ±180° angles of attack (AoA).

The following assumptions were used when creating the numerical models of both tails:

- The NACA 0012 behaves symmetrically about the 90° and -90° AoA,
- The magnitude of the lift coefficient of the NACA 0012 airfoil at 175° AoA was said to be equal to the lift coefficient at 5° AoA,
- The magnitude of the tails' lift coefficients (C_L) were limited to a magnitude of 2 and phased out approaching 90° AoA, while a flat plate drag coefficient ($C_{D,p}$) of 2 was phased in approaching 90° AoA,
- Three-dimensional flow between the vertical and horizontal tails was not taken into consideration due to lack of wind tunnel data,
- The coordinate system used followed the traditional right-hand rule with positive X out the nose and positive Y out the right side of the helicopter. Both tails were modeled after the methods found in Helicopter Performance, Stability, and Control (Prouty, 2002).

The vertical tail was also said to only be affected by the freestream velocity, aircraft body-rates, and the sidewash (η_{tv}) of the tail rotor. The following parameters were passed from the HeloForceMoment module into VerticalEmpennage: the state vector (u), the array composed of thirteen (13) parameters, and the density (ρ).

The state vector was composed of body angles, body velocities, body rates, and control positions. The state vector can be seen below:

u = (Phi, Theta, Psi, Vx, Vy, Vz, p, q, r, theta0m, B1, A1, theta0t)

The VerticalEmpennage module, after reading in the state vector, calculated the effective velocities in both the Y (Y_{effv}) and the Z (Z_{effv}) directions. The lengths of the moment arm in the X (L_{xv}) and Z (L_{zv}) directions were used in Equation 3.9.1 and Equation 3.9.2 (Note: all subscripts not exactly the same as used in the MATLAB program):

$$Y_{effv} = -r \times L_{xv} + p \times L_{zv} + V_y \qquad \text{Equation 3.9.1}$$

$$Z_{effv} = q \times L_{xv} + V_z \qquad \text{Equation 3.9.2}$$

Next, the total velocity (V_v) was calculated with the effective velocities and the X velocity (V_x) as seen in Equation 3.9.3 and was limited to not be any less than 0.001 in value in the VerticalEmpennage module:

$$V_v = \sqrt{V_x^2 + Y_{effv}^2 + Z_{effv}^2} \qquad \text{Equation 3.9.3}$$

The dynamic pressure (Q) was calculated with density (ρ) and velocity (V_v) as seen in Equation 3.9.4:

$$Q = \left(\frac{1}{2}\right)\rho V_v^2 \qquad \text{Equation 3.9.4}$$

Alpha (α) and beta (β) were then calculated in Equation 3.9.5 and Equation 3.9.6 with respect to the nose of the helicopter being 0° and beta being positive in sign from the right side of the pilot (Note: that the atan2 function finds the arctan of the two values and the coordinate system in which they form the angle):

$$\alpha = a\tan 2\left(Z_{effv}, V_x\right) \qquad \text{Equation 3.9.5}$$

$$\beta = a\tan 2\left(Y_{effv}, V_x\right) \qquad \text{Equation 3.9.6}$$

The sidewash angle (η_{tv}) from the tail rotor on the vertical tail was calculated with the ratio of dynamic pressure of the vertical tail to freestream (q_v/q) and the tail rotor disc loading (DL_t) as seen in Equation 3.9.7. The sidewash angle was limited to 5°:

$$\eta_{tv} = \left[\frac{DL_t}{4(q_v/q)Q}\right] \qquad \text{Equation 3.9.7}$$

The contributing adjustments to sideslip (vertical tail AoA) were then summed into a total beta (β_{totalv}) in Equation 3.9.8, followed by the calculation of the lift coefficient for the vertical tail (C_{Lv}), which was limited to ±2 in Equation 3.9.9. The vertical tail incidence (i_v) was denoted positive leading edge to the right and the lift-slope curve ($C_{L\alpha}$) was also used to calculate C_{Lv}:

$$\beta_{totalv} = \eta_{tv} - i_v + \beta \qquad \text{Equation 3.9.8}$$

$$C_{Lv} = -C_{L\alpha}\sin\left(\beta_{totalv}\right) \qquad \text{Equation 3.9.9}$$

The drag coefficient (C_{Dv}) on the vertical tail was then calculated with the profile drag of the vertical tail (c_d) and the span efficiency factor (e) as seen in Equation 3.9.10:

$$C_{Dv} = \underbrace{\left[\frac{C_{Lv}^2}{\Pi e AR}\right]}_{induced} + \underbrace{c_d}_{profile} + \underbrace{2\left|\sin(\beta_{totalv})\right|}_{flatplate} \qquad \text{Equation 3.9.10}$$

Lift (L_v) and drag (D_v) were calculated with the area of the vertical tail (A_v) in Equation 3.9.11 and Equation 3.9.12:

$$L_v = (q_v / q) A_v Q C_{Lv} \qquad \text{Equation 3.9.11}$$

$$D_v = (q_v / q) A_v Q C_{Dv} \qquad \text{Equation 3.9.12}$$

Next the forces X_v, Y_v, and Z_v the vertical tail produced were calculated with Equation 3.9.13 and Equation 3.9.15:

$$X_v = if\left[-\Pi/2 < \beta_{totalv} < \Pi/2\right]\left(-L_v \sin(\beta_{totalv}) - D_v \cos(\beta_{totalv})\right) \qquad \text{Equation 3.9.13}$$
$$= else\left(L_v \sin(\beta_{totalv}) - D_v \cos(\beta_{totalv})\right)$$

$$Y_v = if\left[-\Pi/2 < \beta_{totalv} < \Pi/2\right]\left(L_v \cos(\beta_{totalv}) - D_v \sin(\beta_{totalv})\right) \qquad \text{Equation 3.9.14}$$
$$= else\left(-L_v \cos(\beta_{totalv}) - D_v \sin(\beta_{totalv})\right)$$

$$Z_v = \left(-D_v \cos(\alpha_v)\right) \qquad \text{Equation 2.7.15}$$

Finally the moments L_v, M_v, and N_v that the vertical tail created were calculated with Equation 3.9.16 through Equation 3.9.18:

$$L_v = Y_v L_{zv} \qquad \text{Equation 3.9.16}$$

$$M_v = Z_v L_{xv} - X_v L_{zv} \qquad \text{Equation 3.9.17}$$

$$N_v = -Y_v L_{xv} \qquad \text{Equation 3.9.18}$$

The forces and moments of the VerticalEmpennage are then returned to the HeloForceMoment module for summation with the rest of the helicopter modules, which concludes the mechanics of the vertical empennage.

The HorizontalEmpennage module for the horizontal tail was created in the same sense as the VerticalEmpennage. The effective velocities were then calculated for the horizontal tail in Equation 3.9.19 and Equation 3.9.20:

$$Y_{effh} = -rL_{xh} + pL_{zv} + V_y \qquad \text{Equation 3.9.19}$$

$$Z_{effh} = qL_{xh} + V_z \qquad \text{Equation 3.9.20}$$

The total velocity (V_h) and the dynamic pressure (q) were calculated for the horizontal tail as was for the vertical tail. Alpha (α_h) and beta (β_h) were then calculated in the same way as for the vertical tail, with positive beta being off to the right side of the pilot. Next, the main rotor downwash angle (η_{mh}) and was calculated based on main rotor disc loading (DL_m) and the ratio of horizontal velocity to freestream velocity (v_h/v_1) as seen in Equation 3.9.21:

$$\eta_{mh} = \left[\frac{DL_m(v_h / v_1)}{4Q}\right] \qquad \text{Equation 3.9.21}$$

The main rotor downwash angle was limited to 90°, which will be when the helicopter is in near hover. This was done due to the fact that if dynamic pressure goes to zero (0) the main rotor downwash angle will go to infinity. Total alpha (α_{totalh}) and the lift horizontal coefficient (C_{Lh}) were calculated with Equation 3.9.22 and Equation 3.9.23:

$$\alpha_{totalh} = -\eta_{mh} + i_h + \alpha_h \qquad \text{Equation 3.9.22}$$

$$C_{Lh} = C_{L\alpha}\sin(\alpha_{totalh}) \qquad \text{Equation 3.9.23}$$

The drag coefficient (C_{Dv}) on the horizontal tail was then calculated with the profile drag of the vertical tail (c_d) and the span efficiency factor (e) in the same way as the vertical tail drag coefficient did, but using alpha total instead. Lift (L_h) and drag (D_h) were calculated with the area of the vertical tail (A_h), which was also calculated in the same way as the vertical tail.

Next the forces X_h, Y_h, and Z_h the horizontal tail produced were calculated with Equations 3.9.24-3.9.26:

$$X_h = if\left[-\Pi/2 < \alpha_{totalh} < \Pi/2\right]\left(L_h\sin(\alpha_{totalh}) - D_h\cos(\alpha_{totalh})\right) \qquad \text{Equation 3.9.24}$$
$$= else\left(-L_h\sin(\alpha_{totalh}) - D_h\cos(\alpha_{totalh})\right)$$

$$Y_v = \left(-D_h\cos(\beta)\right) \qquad \text{Equation 3.9.25}$$

$$Z_h = if\left[-\Pi/2 < \alpha_{totalh} < \Pi/2\right]\left(-L_h\cos(\alpha_{totalh}) - D_h\sin(\alpha_{totalh})\right) \qquad \text{Equation 3.9.26}$$
$$= else\left(L_h\cos(\alpha_{totalh}) - D_h\sin(\alpha_{totalh})\right)$$

Finally the moments L_h, M_h, and N_h that the vertical tail created were calculated with Equations 2.7.16-2.7.18:

$$L_v = Z_h L_{yh} \qquad \text{Equation 3.9.27}$$

$$M_h = Z_h L_{xh} - X_h L_{zh}$$ Equation 3.9.28

$$N_h = -Y_h L_{xh}$$ Equation 3.9.29

The forces and moments of the HorizontalEmpennage are then returned to the HeloForceMoment module for summation with the rest of the helicopter modules, which concludes the mechanics of the horizontal empennage.

4.0 CONCLUSSIONS AND RECOMMENDATIONS

After the completion of all the MATLAB modules, IA then tested each module to determine whether or not all the modules worked accordingly. The values produced by each module were compared against Excel spreadsheets that were created by members of IA during AE 421.

Several assumptions were used to create the flight modules. The greatest of these assumptions was that all aero coefficients were based off of historical trends. In order to produce an accurate model, IA recommends that a detailed wind tunnel model be produced in order to determine accurate aero coefficient data.

Many of the problems encountered during this independent study occurred during the creation of the forward flight module. After the first completion, the module was executed. The calculations produced thrust and torque values higher than anticipated. Much time was spent in the debugging process of this module. After several modifications, it was determined that the there were errors in the initial Excel spreadsheet. These errors were corrected by modifying the formula used to calculate the angle of attack with respect to the main rotor blades. Once this correction was made, the Excel values were then compared against the MATLAB values. The percent difference was four (4) percent error with the MATLAB values higher than the Excel values for thrust and torque. IA concludes that his difference was within acceptable limits.

Another problem encountered was during the compilation of all the flight modules. Members of IA would frequently switch between radians and degrees. This was done because of personal preference - degrees were easier to work with when conducting calculations. However, the programs used (i.e., MATLAB and Excel), handled trigonometric functions in radians, not degrees. This toggling between radians and degrees caused many errors because IA members would often forget to switch between either radians or degrees.

IA also attempted to compile the flight modules into Flight Gear. However, little success was achieved. It was concluded that this was most likely due to the fact that the Flight Gear code was written for a Linux operating system. Embry-Riddle Aeronautical University, however, does not operate a Linux-based system. Instead, it operates Windows 2000 for their primary operating system. IA's recommends that the compilation of future flight modules be done in the same operating system as the simulation software.

A more accurate solution where each force and moment was affected by all six controlling variables was attempted. However, due to the time constraint and the complexity of the solution, a fully fleshed out six-by-six matrix was never completed. IA recommends that future students attempt this analysis in order to create a more accurate calculation of the forces and moments experience by the E-21.

Also, the empennage is able to return forces and moments while being able to calculate the effects of the helicopter's body rates. However, this module was limited due to the fact that there was little available information on NACA 0012 airfoils at high angles of attack. IA believes that if more information on high angles of the NACA 0012 airfoil were available, more accurate results would have been achieved. It is recommended that thorough wind tunnel testing be done on the NACA 0012 airfoil in order to gain the information needed for the high angles of attack.

5.0 REFERENCES

Eight to One Aerospace (ETOA). (2003b). AE 420 Aircraft Design Report: Final Preliminary Design of the E-21 HAMR. (AE420 Unpublished Technical Report). Prescott, AZ: Embry-Riddle Aeronautical University.

Prouty, Raymond W. (2002). Helicopter Performance, Stability, and Control. Malabar, Florida: Kreiger Publishing Company.

US Standard Atmosphere, 1976. Accessed on 27 April 2004. <http://scipp.ucsc.edu/outreach/ballon/atoms/1976%20Standard%20Atmosphere.htm>.

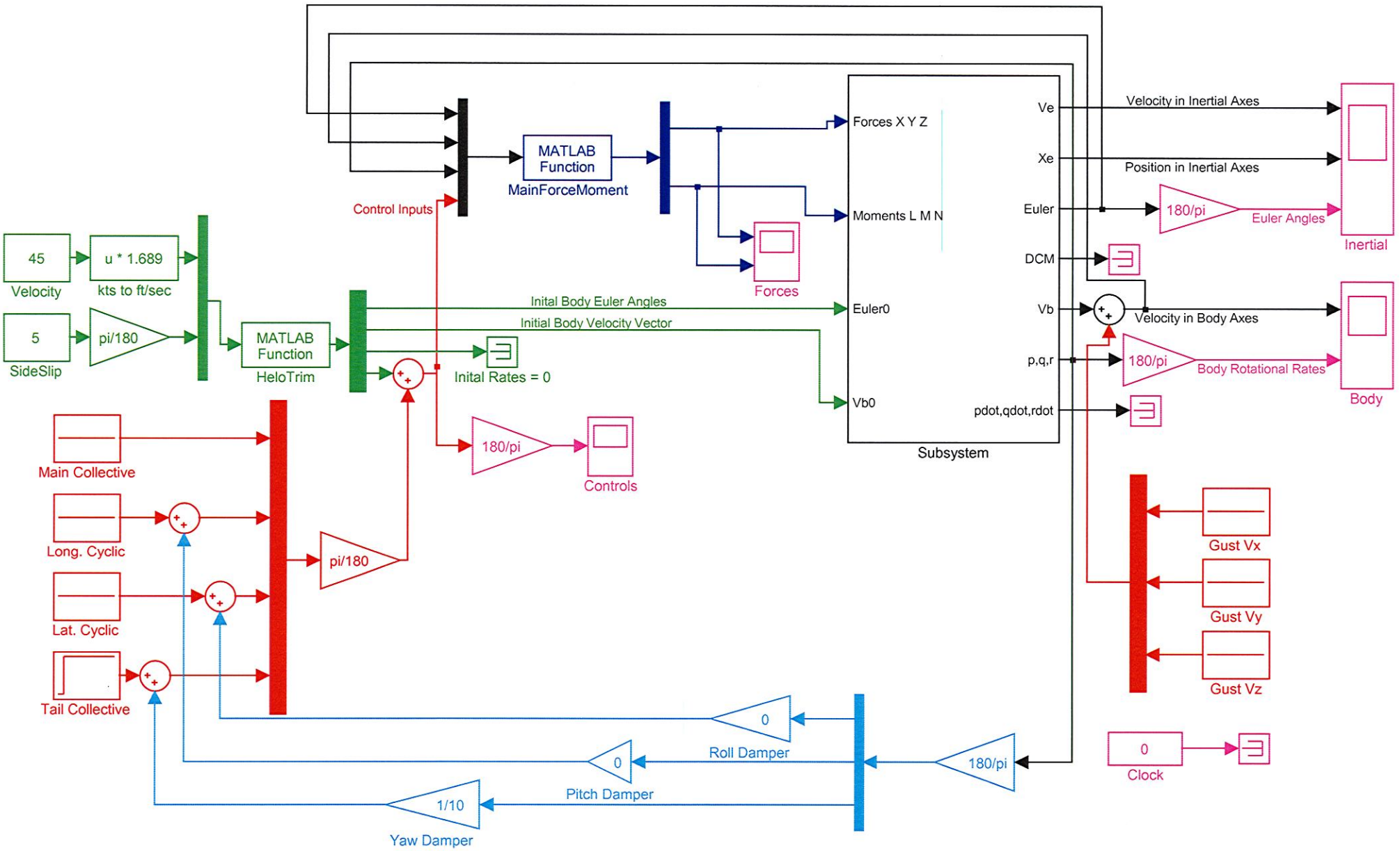
MATLAB Function
MainForceMoment
Control Inputs
Forces
Forces X Y Z
Moments L M N
Euler0
Vb0
Ve
Xe
Euler
DCM
Vb
p,q,r
pdot,qdot,rdot
Subsystem
Velocity in Inertial Axes
Position in Inertial Axes
180/pi
Euler Angles
Inertial
Velocity in Body Axes
Body Rotational Rates
Body
45
Velocity
u * 1.689
kts to fts/sec
5
SideSlip
pi/180
MATLAB Function
HeloTrim
Inital Body Euler Angles
Initial Body Velocity Vector
Inital Rates = 0
180/pi
Controls
Main Collective
Long. Cyclic
Lat. Cyclic
Tail Collective
pi/180
Gust Vx
Gust Vy
Gust Vz
0
Roll Damper
0
Pitch Damper
1/10
Yaw Damper
180/pi
0
Clock